18

Histograms: Volumetric Analysis[1]

Paul Tofts and Gerard Davies
Department of Medical Physics, NMR Research Unit, Institute of Neurology, University College London, Queen Square, London WC4N 3B9, UK

Jamshid Dehmeshki
Medicsight, 46 Berkeley Square, London W1J SAT, UK

18.1 INTRODUCTION

Histograms of MR parameter values measured in the whole brain are increasingly being used to characterize subtle disease that affects large parts of the brain. The histogram is a frequency distribution showing the number of voxels with a particular range of MR parameter values. The most common application of histograms has been to characterize MTR values in the whole brain (Figure 18.1). However the concept is equally

[1] Reviewed by Stefan C.A. Steens, Department of Radiology, Leiden University Medical Center, Leiden, The Netherlands, McGowan.

Quantitative MRI of the Brain. Edited by Paul Tofts
 ISBN: 0-470-84721-2

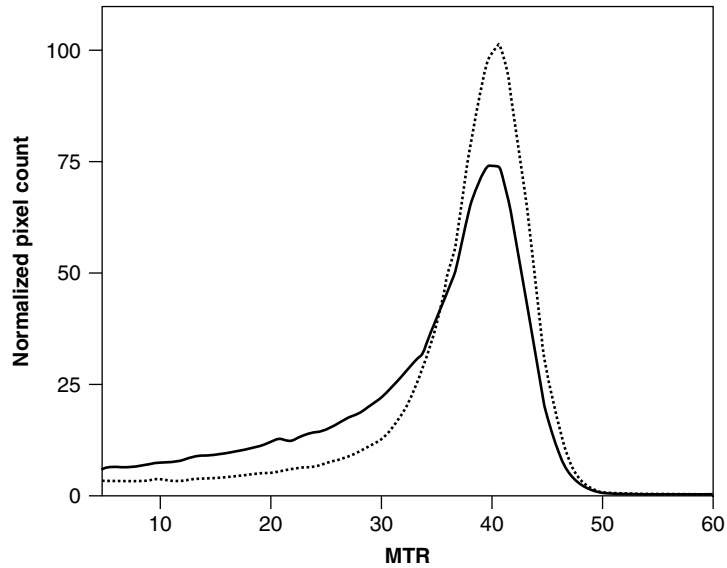

Figure 18.1. The first published whole-brain histograms, from a healthy subject (dotted line) and a patient with MS (solid line). There is a dramatic decrease in voxels at normal MTR values (about 40 pu for this study), and an increase in voxels at lower MTR values. Reproduced with permission from (van Buchem, M.A., Udupa, J.K., McGowan, J.C., Miki, Y., Heyning, F.H., Boncoeur-Martel, M.P., Kolson, D.L., Polansky, M., and Grossman, R.I., Global volumetric estimation of disease burden in multiple sclerosis based on magnetization transfer imaging, in *AM. J. Neuroradiol.*, Copyright 1997 American Society of Neuroradiology

applicable to any intensive parameter that may be affected by diffuse global changes in the brain, and histograms are now being used for other parameters (e.g. diffusion; Figures 18.2 and Figure 18.3).

Why use histograms?

- A measure is obtained (often from the whole brain) that is sensitive to subtle diffuse disease.
- No ROIs need be generated.
- Repositioning on repeat scans is unnecessary.

What are the downsides to histograms?

- Localized changes may not be detected.
- Software is needed to segment the brain and generate the histogram.
- Brain atrophy is a potential confounder.

What kinds of histogram are there?

- VPB (voxels per bin) are absolute histograms showing voxel counts.
- MPX (ml per x-unit) histograms show the volume per x-unit, independent of bin width.
- Partly normalized histograms correct for brain volume, but depend on bin width.
- Fully normalized histograms correct for brain volume and are independent of bin width.

What is the future?

- A standardized approach to normalization will improve inter-centre agreement.
- Broadening of MTR and T_1 histograms by transmit non-uniformity will be reduced.
- Sophisticated global histogram analysis methods (PCA and LDA) will enable individual patients to be classified and monitored.

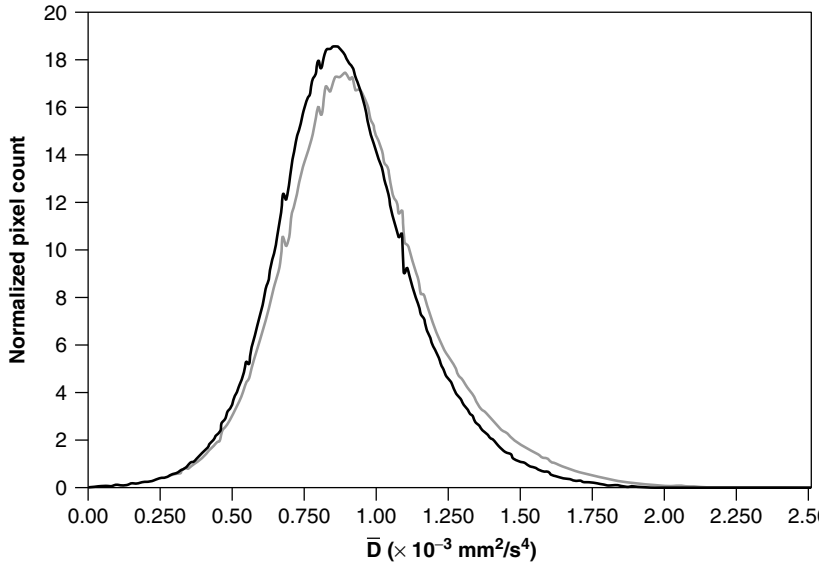

Figure 18.2. Mean ADC histograms from 10 central 5 mm brain slices. Black line, normals; grey line, MS patients. The MS peak is shifted to higher ADC values, and is lower. Discontinuities (histogram spikes) are visible at several values of mean diffusivity, $\overline{D}$; the cause and solution are discussed in Section 18.4.1. Reproduced with permission from Cercignani, M., Iannucci, G., Rocca, M.A., Comi, G., Horsfield, M.A. and Filippi, M., Pathologic damage in MS assessed by diffusion-weighted and magnetization transfer MRI, in *Neurology*. **54**, 1139–1144, Copyright 2000 Lippincott, Williams and Wilkins

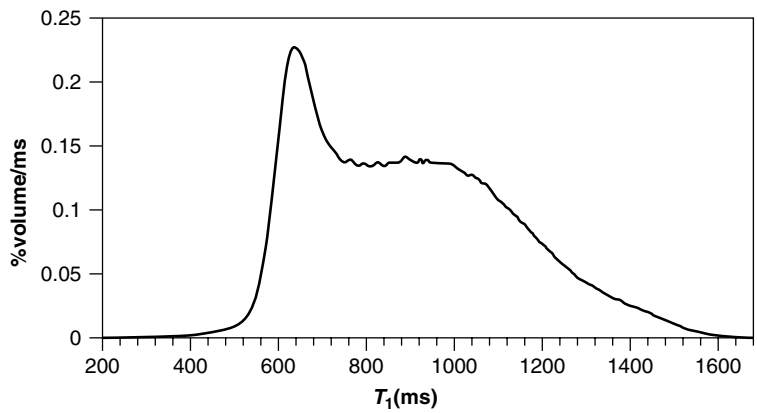

Figure 18.3. A T_1 histogram of the brain. The bin width is 1 ms; and an 11 ms median smoothing filter was applied. White matter has a narrow peak at 640 ms; a secondary peak, from grey matter, is visible at 920 ms. Image de-spiking was used to avoid narrow spikes appearing in the histogram (see Section 18.4.1). T_1 values were calculated using the Parker method that takes account of RF non-uniformity and imperfect slice profile (Parker *et al*., 2001). This histogram shows more structure than MTR or $\overline{D}$ (Figures 18.1 and 18.2), because (i) the intrinsic T_1 values of white and grey matter differ more than their MTR or $\overline{D}$ values do, and (ii) the T_1 values are accurate throughout the brain and the histogram is not broadened by non-uniformity (figure reproduced courtesy of Dr Dan Tozer)

Histogram analysis (where the whole brain is usually tested) avoids any bias or pre-judgment about which parts of the brain may be affected by disease. It also avoids the need to place ROIs on the images. In serial studies it avoids the need to reposition the ROIs in exactly the same location in subsequent images. However if the effects of disease are localized to only part of the brain (for example in visible lesions), then sensitivity to change will be reduced. The example of MS is interesting; initially it was thought that the visible lesions (seen on conventional T_2-weighted MRI) were the key biological features. Now it is recognized that the normal-appearing white matter plays a crucial role, and that whole-brain measures may be at least as sensitive as those derived from lesions in characterizing the course of the disease and its response to treatment. The changes in MR parameter values observed in the normal-appearing brain, where there are no visible lesions, are subtle and care is needed in data acquisition in order that these small changes are not masked by instrumental imperfections. For example the changes seen in MTR histograms are of the order of 1 pu,[2] which is much less than the typical inter-scanner difference (see Chapter 8).

In histogram analysis, any information on the *location* of abnormalities is lost. It may be seen as the extreme antithesis of ROI analysis, where location information is preserved, only certain locations can be tested for change, there is the danger of bias in selecting those locations (and missing significant change in other locations), and if many locations are tested then the Bonferroni correction leads to a loss of sensitivity. A mid-course between histogram and ROI analysis may be voxel-based morphometry,[3] where a relatively limited number of ROIs, that cover the whole brain without bias, are tested.

The first MTR histograms were published by van Buchem and colleagues at Philadelphia (van Buchem *et al*., 1996), derived from MTR maps. Only five central slices (covering a 2.5 cm thick slab) were used, and segmentation[4] was not carried out. A 5 pu cut-off was used. A subsequent whole brain study (van Buchem *et al*., 1997) used segmentation (three-dimensional viewnix) and showed a substantial change in MS – see Figure 18.1. In this chapter the principles of histogram generation are given, with new material on dealing with bin width correctly, on histogram smoothing and on spike removal, and clinical examples are given.

18.2 PRINCIPLES OF HISTOGRAM GENERATION AND ANALYSIS

MR data are collected and the appropriate maps formed (for example MTR, mean diffusivity or T_1). To avoid histogram spikes, the MR images should first be made *pseudo-continuous* (de-spiked) before calculation of the map (see Figure 18.3 and Section 18.4).

The image data are *segmented* to identify the outline of the brain or other tissue (for example white matter or a large tumour) that is being used to generate the histogram. An *absolute histogram* is generated (see Figure 18.6); this shows the number of voxels per unit interval of the MR parameter (e.g. MTR). The interval, or *bin width*, is chosen to divide the range of parameter values into a convenient number of intervals (typically 100; this is discussed further in Section 18.4). The amount of brain volume per unit interval of MR parameter is also easily available, since the volume of a voxel is known. The area under this curve is the total number of voxels (and equivalent to the total brain volume).

Since brain volumes vary greatly between individuals, the histogram is usually *normalized* by dividing all the values by the total number of voxels. A frequency distribution is then obtained. This shows the fraction of the total brain volume that lies in unit interval[5] of the MR parameter (see Figure 18.7).

[2] All MTR values are presented in *percent units* (pu). This avoids the confusion that can arise if MTR is presented without units or in % (Barker *et al*., 1996).

[3] Voxel based morphometry (VBM) is also demonstrated in Chapter 15.

[4] *Segmentation* of an image means generating an outline, or mask, that defines which pixels are within a structure such as the brain, and which are outside.

[5] Provided the bin width value is included in the normalization – see Section 18.4.

Histogram *features* (i.e. *summary parameters*) are calculated, to reduce the information in the histogram down to a few parameters that are intended to contain the important information in the histogram. Typical conventional features are peak height, peak location, mean parameter value; fitted curve parameters and eigenvectors calculated using advanced techniques (principle component analysis and linear discriminant analysis) can also be calculated – see Section 18.4.

The features can then be used to look for differences between groups of subjects. If the separation between groups is sufficiently good, individual subjects can be classified on the basis of their parameter value. Longitudinal changes of parameter value with time may show disease progression or the arrest of the disease process (either spontaneously or by a treatment).

18.3 BIOLOGICAL ORIGIN OF HISTOGRAM CHANGES

Whole-brain histograms are sensitive to diffuse changes in large volumes of tissue (as distinct from focal changes which radiologically are usually visibly obvious and reported as 'lesions'). They can be made for any MRI parameter that may be subtly altered by the presence of diffuse disease. They can detect small changes in parameter value (down to about 1 % of its normal value – see Figures 18.2, 18.4 and 18.13), partly because a large number of voxels are averaged together (thus reducing the effect of noise), and partly because segmentation and repositioning issues are less crucial than in ROI analysis (although the removal of CSF and sensitivity to atrophy remain problems). In a smaller volume such as a lesion it would be very hard to achieve such a good sensitivity. The particular biological changes that are thought to occur in subtle diffuse disease are discussed in Section 18.6, in the chapter ocn each MR parameter (e.g. Chapter 8 for MTR), and in Chapter 14 on biology. In large lesions (particularly tumours), histogram analysis may be helpful, particularly if they are heterogeneous and a simple mean value would not be appropriate, although the result may be sensitive to the segmentation procedure. Small alterations to the ROI used to define the voxels to be included in the histogram may have a large effect on the histogram features, particularly if the lesion has heterogeneous structure near its edge.

The peak location (mode) corresponds to the parameter value that is most common in the brain tissue. It is closely related to the mean value (although not the same, particularly for asymmetric histograms). If normal tissue is homogeneous, the peak can be very well defined (see Figure 18.1). A shift in peak location in disease may occur if a large number of voxels are affected; alternatively, the peak may stay at the same location but be depressed in height as a large volume of tissue acquires abnormal values of the parameter (as in MS – Figure 18.1). Because the histograms are usually normalized to have fixed area, a broadening of the histogram necessarily reduces its peak height.

18.4 QUANTIFICATION OF HISTOGRAMS – PRACTICAL DETAILS

In Section 18.2 the principles of histogram generation were given – here we give more details of practical implementation. Once the basic voxels-per-bin histogram has been produced, the remainder of the operations can often be carried out on a personal computer using spreadsheet software. Section 18.5 will describe difficulties that can arise, particularly in multicentre comparisons.

18.4.1 Data Acquisition

The image data are acquired taking into account:

- Good practice in obtaining accurate values of the MR parameter in question (e.g. MTR, Chapter 8, diffusion, Chapter 7, or T_1, Chapter 5). In MTR studies, small changes in peak location may be significant, and therefore attention to data collection techniques is important. The parameter value in an ROI placed in white matter should be checked for accuracy, if possible by comparison with published data known to be accurate.

- Smaller voxels will give fewer partial volume errors (see following section on segmentation), although at the expense of noise.
- The *parameter maps* are calculated from MR images. The images must be made pseudo-continuous (i.e. de-spiked) before calculation of the maps, and the maps must be stored at sufficient resolution.

18.4.1.1 Image De-spiking

To avoid the generation of discontinuities in the histogram of the calculated map values (e.g. MTR), the image data must be made as continuous a possible. Each image variable, although represented as a floating-point number in the computer, at the time of division, can only have a finite number of values (since it derives from an integer image, typically 12-bit, in the MR imager). Typically the maximum image intensity is 1000. Its distribution can be thought of as a series of spikes (at integer values), rather than the continuous distribution it has physically. The continuously variable value has been forced to one of the two nearest integer values. The shift (of up to 0.5 x-units) may be small compared with the noise in an image, and may thus have been considered unimportant until histograms arrived. Division of two spiked distributions produces a quotient distribution that also has discontinuities in it (see Figures 18.2, 18.6 and 18.8). The artefact can be avoided by adding random noise to each floating-point image value, before division. The noise is evenly distributed between -0.5 and $+0.5$, and has the effect of forcing the image values to have almost continuous (pseudo-continuous) distributions. Having de-spiked the original images, the resulting distribution in the quotient is also continuous. Figure 18.3 shows an example of the successful use of this de-spiking algorithm.

18.4.1.2 Map Resolution

After calculation of the map parameter value (e.g. MTR) as a floating point number, it is stored in integer form for space reasons. Scaling of the values is usually necessary before conversion to integers. (Thus for MTR, a resolution of 1 pu is not sufficient, and the values should be multiplied by 10 before being converted to integers – see Table 18.1).

18.4.2 Image Segmentation

The segmentation process should be reproducible, accurate and as independent of any human judgment as possible. Volume measurement, which necessarily involves segmentation, has been described in Chapter 16. Defining the outline of the whole brain is in principle easy, particularly from T_1-weighted images. The lower edge of the brain, where it merges into the spinal cord, has to be defined in some clear way. The hardest issue is how to deal with partial volume voxels, i.e. those that contain a mixture of brain and CSF. Various strategies have been used; Dehmeshki (Dehmeshki *et al*., 2002a) has rejected voxels that contain less than a given proportion of brain tissue (typically 80 %). The difficulty is that there is a large volume of brain, particularly grey matter, that is adjacent to (and shares voxels with) a different tissue, and an overstrict criterion will reject large amounts of brain tissue which may be biologically relevant in evaluating the effect of disease (although the remaining voxels are at least known to be pure). Another approach is to be strict in rejecting CSF, then more lax in separating grey and white matter.[6] When it comes to creating individual histograms of grey and white matter, partial volume voxels become even more important, since a large proportion of the grey matter lies in voxels that contain CSF. From a practical point of view, it has to be accepted that whole-brain histograms will always have a small contribution from CSF, and that provided the segmentation is carried out in a consistent manner this need not be a problem. However the interpretation of histogram changes can be equivocal, since atrophy will alter the contribution of partial volume voxels to the histogram.

The segmentation should be carried out on a plain PD-, T_1- or T_2-image dataset that has

[6] Stefan Steens, private communication.

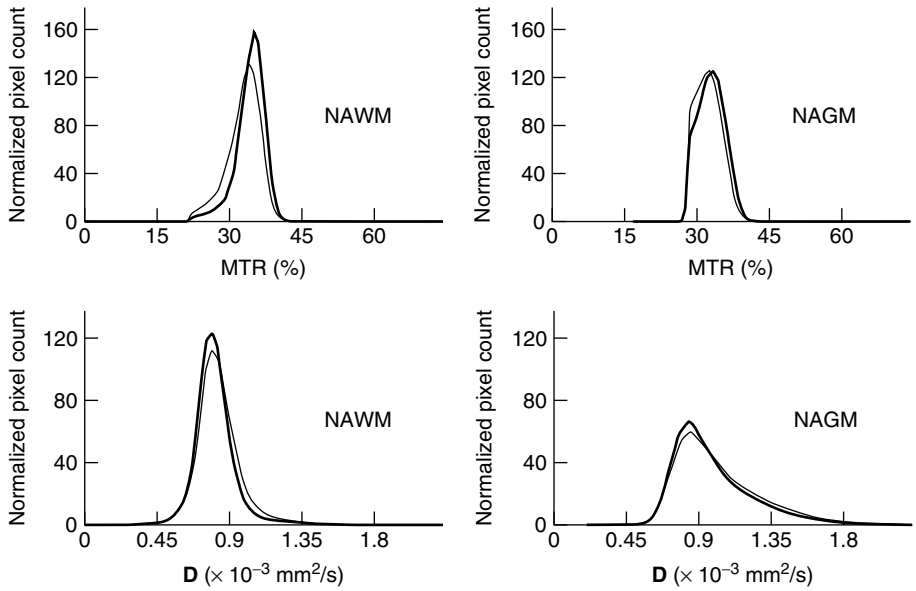

Figure 18.4. Histograms of MTR and mean diffusivity MD from normal-appearing white and grey matter (NAWM, NAGM). Black line, normals; grey line, MS patients. Segmentation was carried out on fractional anisotropy maps (from diffusion tensor images). Note the narrowness of the MTR histogram in white matter, and the absence of low MTR voxels that would be partly occupied by CSF. Reproduced with permission from Cercignani, M., Bozzali, M., Iannucci, G., Comi, G., and Filippi, M., Magnetization transfer ratio and mean diffusivity of normal appearing white and grey matter from patients with multiple sclerosis, in *J. Neorol•. Neurosurg. Psychiat.*, Copyright 2001 BMJ Publishing Group)

different weighting from that used to generate the parameter map of interest. For example if an MTR histogram is being generated, the segmentation process should (ideally) not use any MTR-weighted image data (otherwise a change in MTR value would alter the segmentation). Thus using a 5 or 10 pu cut-off, which is bringing MTR information into the segmentation process, is to be avoided if possible. Low MTR value pixels, such as those in CSF, should be removed by explicit segmentation in a different image. If the segmentation is successful, there will be very few low-MTR voxels in the histogram. The range of segmentation techniques used in published work, sometimes not clearly defined, can be judged from the differing appearance of the low-MTR tails in Figures 18.1, 18.4, 18.5 and 18.7. If normal-appearing brain is to be studied, lesions will first have to be identified and removed (Tortorella *et al*., 2000).

18.4.3 Generation of Absolute Histogram

The *bin width* Δ is chosen, such that the range of parameter (x-) values is divided up into a reasonable range of bins. Too few bins will result in important structure being obscured by the smoothing effect of a wide bin (see Figure 18.5) and the determination of features, particularly those that involve identifying the peak, will be unreliable (this can be partly rectified by interpolation – see Section 18.5.6 and Figure 18.12). Too many bins will result in each bin being noisy (since the number of voxels in each bin will be small) and also the resulting large datasets may become unwieldy. However the histogram can be smoothed (see Figure 18.8), and it is better to have too many bins than too few.

For global feature extraction methods such as LDA (see Section 18.4.9) using a large number of

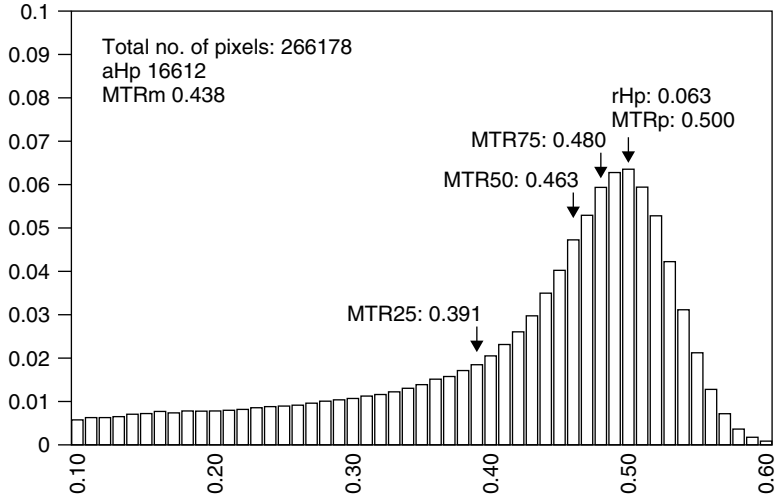

Figure 18.5. A rare example of a histogram shown as a bar chart, rather than a continuous function. Each bin is shown explicitly. The percentile parameters (e.g. MTR25) show sub-bin resolution, implying some (unstated) interpolation, although the peak location (stated as 50 pu) seems to have suffered from a rounding error. Reproduced with permission from van Waesberghe, J.H., van Buchem, M.A., Filippi, M. Castelijns, J.A., Rocca, M.A., van der Polman, C.H. and Barkhof, F., MR outcome parameters in multiple sclerosis: comparison of surface-based thresholding segmentation and magnetization transfer ratio histographic analysis in relation to disability (a preliminary note), in *Am. J. Neuroradiol.*, Copyright 1998 American Society of Neuroradiology

bins may give a dataset that is unwieldy, in terms of storage and computing speed requirements, and pre-processing to give larger bins may be appropriate, especially as the particularly histogram structure around the peak is less important.

Often the width used is unity, without an explicit considered choice having been made. For MTR histograms, with a peak width (full-width half-maximum) of around 10 pu, a width of 1 pu is probably too large, and probably contributes error in determining the peak location and height. Conversely, for T_1 histograms (peak width about 700 ms) a bin width of 1 ms is a little small, although smoothing reduces the noise to acceptable levels (see Figure 18.3).

The range of x-values $x_{\min}$–$x_{\max}$ is chosen. Normally the lower value is 0, and the upper value is higher than the highest value present in the parameter values. $x_{\min} - \Delta/2$ must be less than or equal to the lowest value of x present in the set of segmented voxels, and $x_{\max} + \Delta/2$ must be greater than or equal to the highest value present. For convenience $x_{\min}$ and $x_{\max}$ represent the *centre* of the first and last bin, respectively. (With this formalism, if the first bin has a centre value of zero, then the left-hand edge of this bin is negative.)

Sometimes extreme values of x are removed (e.g. low MTR values or high T_1 values), on the grounds that they represent CSF; however this process may affect the normalization, and should properly be carried out as part of segmentation. In any case segmentation should ideally be carried out without regard to the parameter values to avoid bias (see Section 18.4.2 above).

The VPB histogram h^{vpb} is then generated by voxel-counting as follows. The number of bins, N, is

$$N = \frac{(x_{\max} - \mathrm{x}_{\min})}{\Delta} + 1 \qquad (18.1)$$

The ith bin covers the range $x_i{}^-$ to $x_i{}^+$ with its centre at x_i^{c}:

$$x_i{}^- = \mathrm{x}_{\min} + (i - 1.5)\Delta; \quad x_i^c = \mathrm{x}_{\min} + (i - 1)\Delta$$
$$x_i{}^+ = \mathrm{x}_{\min} + (i - 0.5)\Delta \quad (i = 1, N) \qquad (18.2)$$

Table 18.1. An example of histogram generation. MTR values, at 0.1 pu intervals, are multiplied by 10 and stored as integers in the MTR map. A histogram with 0.2 pu bin width is to be generated, from 0–50 pu. The true (floating point) values are recreated from the integer map, by dividing by 10. The centre of the first bin is chosen to be half-way between the values of the first two MTR values, since two values will contribute to each bin; thus, $x_{\min} = 0.15$ pu; $\triangle = 0.2$ pu, $x_{\max} = 49.95$ pu; $N = 250$. The centres and edges can be calculated using Equation (18.2)

MTR value (floating point)	Integer representation	Bin number, i	Bin centre, x_i^c	Left edge of bin, x_i^-	Right edge of bin x_i^+
0.1	1	1	0.15	0.05	0.25
0.2	2				
0.3	3	2	0.35	0.25	0.45
0.4	4				
0.5	5	3	0.55	0.45	0.65
0.6	6				
0.7	7	4	0.75	0.65	0.85
0.8	8				
0.9	9	5	0.95	0.85	1.05
1.0	10				
–	–	–	–	–	–
35.1	351	176	35.15	35.05	35.25
35.2	352				
35.3	353	177	35.35	35.25	35.45
35.4	354				
35.5	355	178	35.55	35.45	35.65
35.6	356				
–	–	–	–	–	–
49.9	499	250	49.95	49.85	50.05
50.0	500				

Note that by choosing the bin centre to lie between the two MTR values, the bin edges then lie *between* MTR values, and the allocation of MTR values to bins is straightforward. (In contrast, if we chose 0.1 pu, 0.3, 0.5,... as the centres of 0.2 pu-wide bins, there would be an ambiguity in allocating the intervening values (0.2 pu, 0.4,...), which would lie on the border between two bins.) If a bin width of 0.1 pu was required, the bin centres would be at 0.1 pu, 0.2 pu,... ($x_{\min} = 0.1$ pu; $\triangle = 0.2$ pu; $x_1^- = 0.05$ pu); if a bin width of 0.3 pu was required, the bin centres would be at 0.2 pu, 0.5 pu,... ($x_{\min} = 0.2$ pu; $\triangle = 0.3$ pu; $x_1^- = 0.05$ pu).

Thus the first bin covers the range $x_{\min} - \Delta/2$ to $x_{\min} + \Delta/2$, and last bin covers $x_{\max} - \Delta/2$ to $x_{\max} + \Delta/2$. An example is given in Table 18.1. Each parameter value in the segmented map is then tested for being in the range for bin i (as defined above); if true then the value h_i^{vpb} for that bin is incremented by 1, and no further test on that voxel is carried out. (This is to avoid problems at bin boundaries where a voxel might qualify for inclusion in two bins.) After classifying all the segmented voxels, we have an absolute histogram h_i^{vpb}, which shows the number of voxels per bin, and where the sum of the values equals the total number of voxels. Examples of voxels-per-bin histograms are shown in Figure 18.6, derived from MTR whole-brain maps.

The MPX histogram, showing the volume per x-unit, has the advantage of being relatively independent of bin width. In Figure 18.6 the VPB is clearly dependent on (and approximately proportional to) the bin width. By using the quantity volume per x-unit (e.g. ml per pu or ml per ms), h_i^{vpx}, we have a measure that is more physically meaningful, that is relatively independent of the particular bin width and voxel size chosen, and that is more easily compared between studies. The

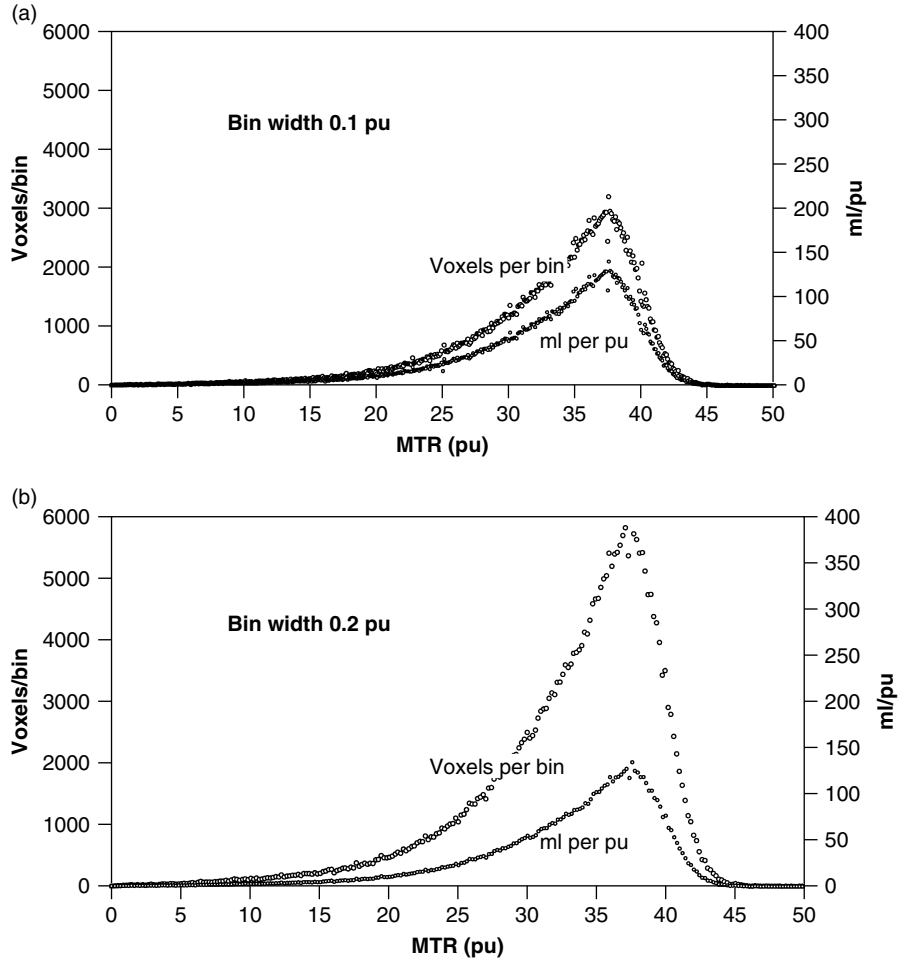

Figure 18.6. Absolute VPB histograms are created by counting the number of voxels in each interval, or *bin*, of MR parameter (in this case MTR); see left-hand axis. There are a total of 311 678 voxels, each of volume 4.4 mm.^{3} By taking account of the bin-width and voxel size, absolute MPX histograms with physically meaningful units (e.g. ml/pu–right-hand axis) can be produced, independent of the bin width. In this subject the peak height is around 130 ml/pu. The approximate full-width half-maximum of the histogram is about 10 pu. The area under the curve can be estimated approximately, treating it as a simple triangle, by multiplying the peak height by the full-width half-maximum, to give 1300 ml (in fact the exact volume is 1370 ml). (a) and (b) show histograms at two different bin widths (0.1 and 0.2 pu). The VPB histogram changes with bin width, whereas the MPX histogram is independent of bin width

histogram value is just obtained by dividing the VPB histogram by the bin width and multiplying by the voxel volume V_{vox}:

$$h_i^{\text{vpx}} = h_i^{\text{vpb}} V_{\text{vox}}/\Delta \qquad (18.3)$$

and examples are given in Figure 18.6.

18.4.4 Normalized Histogram

The *normalized histogram* (corrected for brain size) is calculated as follows. The sum of all the histogram values is calculated. Each histogram value is then divided by this sum, and also by the bin width. The resulting normalized histogram

h then has the property that the area under the histogram is unity. This property is independent of the bin width. The normalized histogram can be calculated from either form of the absolute histogram (either VPB or MPX). For convenience the y-values can be multiplied by 100 %; this gives values that are easier to handle. For example the peak height of a normal MTR histogram is then around 10 % vol/pu (see Figure 18.7).

$$h_i = \frac{100\,\%\, h_i^{\mathrm{vpb}}}{\Delta \sum_i^N h_i^{\mathrm{vpb}}} = \frac{100\,\%\, h_i^{\mathrm{vpx}}}{\Delta \sum_i^N h_i^{\mathrm{vpx}}} \tag{18.4}$$

Histograms calculated in this way [with the factor Δ in as in Equation (18.4)] are relatively

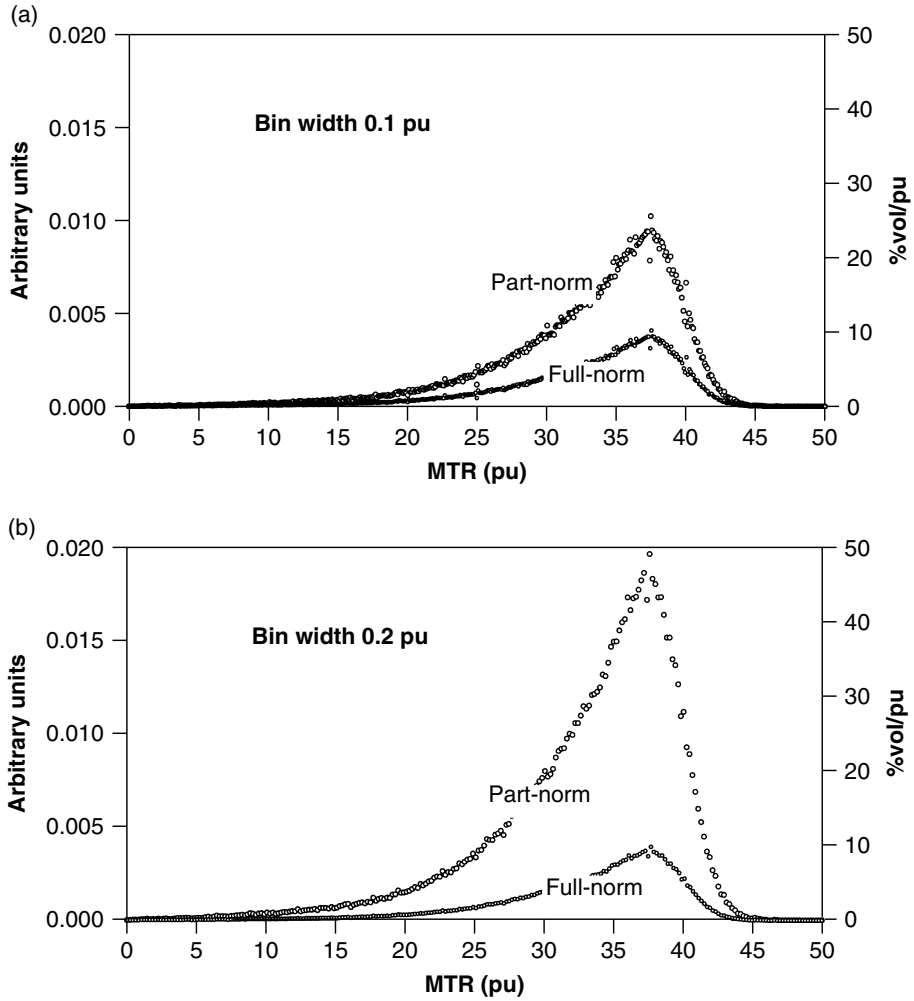

Figure 18.7. Partly normalized and fully normalized MTR histograms. The partly normalized histograms were calculated by dividing each absolute histogram value by the sum of the values (without taking account of bin width); they have a peak height that is dependent on the bin width (in fact inversely proportional to it). The fully normalized histograms were calculated taking account of bin width [Equation (18.4)]; they are independent of bin width, with a peak height of about 10 % vol/pu, a peak width (full-width half-maximum) of 10 pu, and an area of 100 % vol

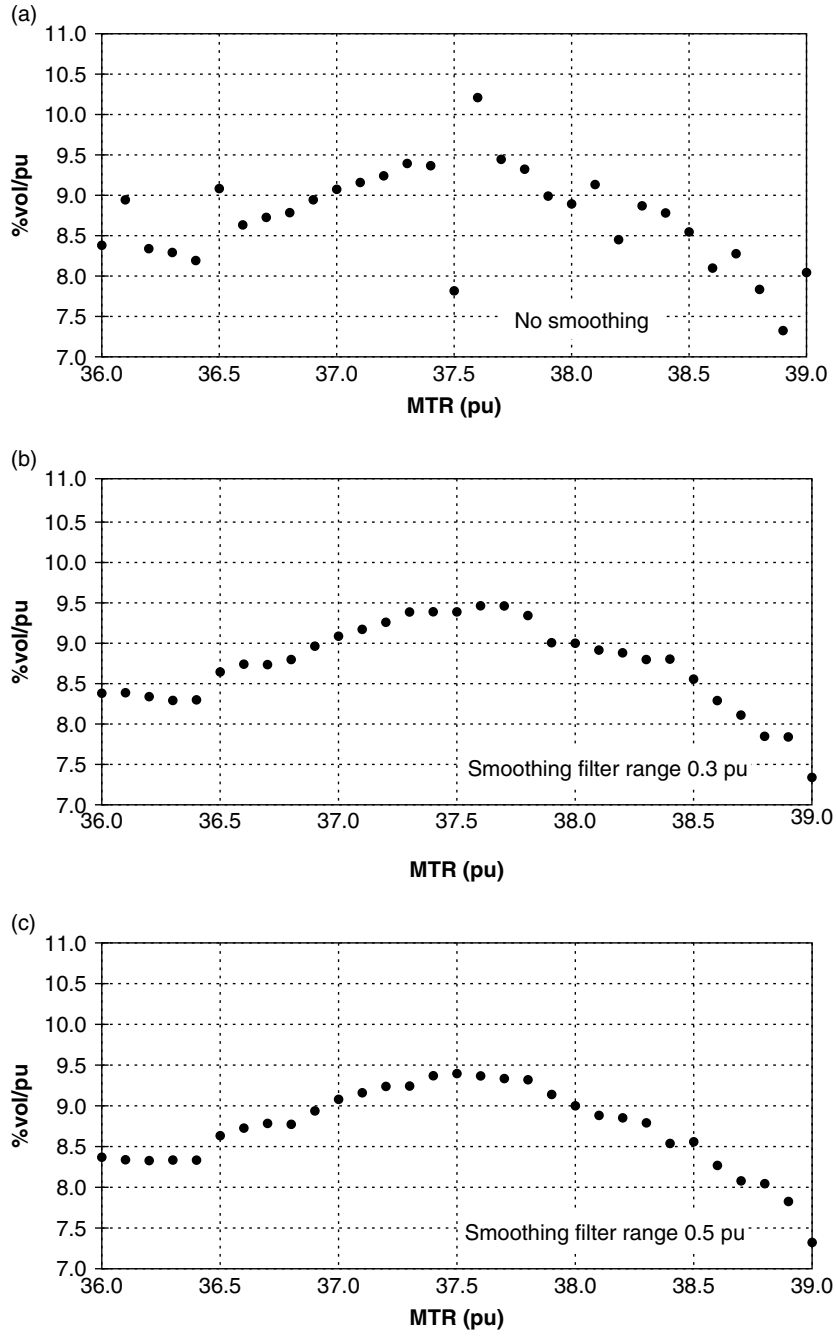

Figure 18.8. The effect of a median smoothing filter on the structure around the peak of the 0.1 pu bin width fully normalized MTR histogram shown in Figure 18.7(a) (right-hand axis). A smoothing range of 0.5 pu means that five bins were used (the centre bin and two neighbours on each side). A 0.3 pu filter has a dramatic effect on the narrow spike at 37.5 and 37.6 pu; a 0.5 pu filter seems optimal in terms of tightening up the distribution of y-values whilst not depressing the peak. The 1.1 pu filter has clearly depressed the peak height

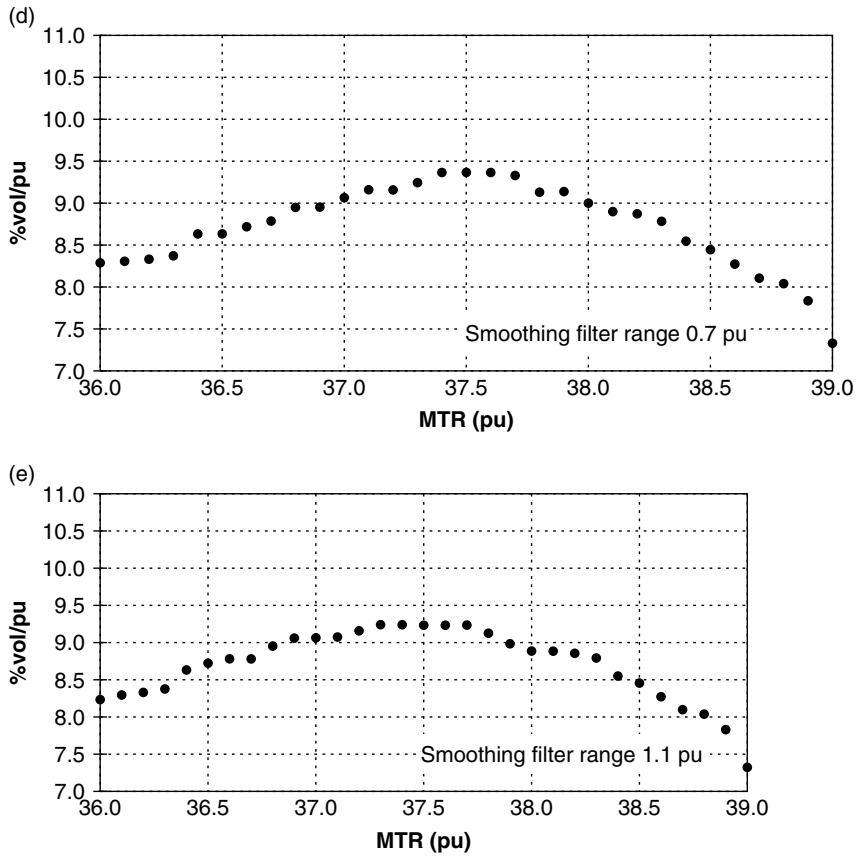

Figure 18.8. (*continued*)

independent of bin width (see fully normalized histogram in Figure 18.7). If division by the bin width is not included, then the y-values are dependent on bin width (see partly normalized histogram in Figure 18.7). If there is an increasing use of bin widths other than 1, and an increasing desire to compare histograms from different sites, it is worthwhile using this form of the histogram, with y-units % vol/pu (for MTR), % vol/ms (for T_1) or 10^9 % vol/m^{2}s (for mean diffusion).

18.4.5 Histogram Smoothing

If the bin width has been chosen to be small enough to preserve structure in the peak, the histogram would probably benefit from some smoothing. An example of progressive smoothing of a high-resolution MTR histogram, using a median[7] filter, is shown in Figure 18.8. The raw histogram, created with bin width 0.1 pu, shows the effect of noise and a spike is also visible. Progressively more smoothing, achieved by increasing the range of the median filter, first reduces the noise then starts to decrease the peak height. A filter range of 0.5 pu seems a good compromise (although 0.3 pu would also be acceptable). This is about 5 % of the peak width (full-width half-maximum about 10 pu), and comparable values are likely to be appropriate for histograms of other MR quantities. For example, the bimodal T_1 histogram in Figure 18.3, where the main peak has a width of

[7] A median filter selects the median value from all the values within its range, and replaces the y-value by that median. It is easily implemented on a spreadsheet.

about 200 ms, responded well to a filter of width 11 ms (5 % of the width). Other additional forms of processing might be used before calculating the features (Section 18.4.7), however these are not recommended. Note that the median filter tends to produce a step-like structure to the histogram if over-used [see Figure 18.8(e)], since only a limited number of results are possible (unlike a linear convolution filter where the results is continuous). Thus very narrow bins might not respond well to median filtering. Table 18.2 summarizes recommended values of bin width and smoothing for the three main types of histogram.

18.4.6 Histogram Display

The appearance of a histogram that is displayed or published can be altered depending on how the basic data are displayed, even though this may not affect the basic data that are used for feature extraction. Although they are categorical, only having values at discrete x-values, they are often shown as continuous, and often with an unstated amount of smoothing. The points may be joined up to form a continuous line; the points themselves may be suppressed, so that only the line is shown. Some form of 'smooth line' may be used, instead of joining up the points. Examination of the options for plotting data in a spreadsheet reveals the large number of choices available. Published histograms can have many different appearances (see Figures 18.1, 18.2, 18.4, 18.5, 18.11 and 18.13). The nature of the underlying data used for the feature extraction is often unclear. The clearest approach seems to be to plot the individual bin-values that were used for analysis (e.g. as in Figure 18.3 or 18.5).

An average histogram from a group of subjects is often presented; a feature extracted from such a group histogram will not have the same value as the mean value of the feature extracted from many individual histograms. For example, the peak location in a group histogram will not (in general) equal the mean peak location measured in the histograms from many individuals.

18.4.7 Unimodal Histogram Features

Unimodal histogram features (i.e. summary parameters) can be calculated, to reduce the information in the histogram down to a few parameters that are intended to contain the important information in the histogram. Typical conventional features that are appropriate for unimodal histograms are peak height, peak location, mean parameter value and centile values (van Buchem *et al*., 1996). Advanced techniques (principle component analysis and linear discriminant analysis (Dehmeshki *et al*., 2002b; see Section 18.9) produce a score which characterizes the whole histogram. Conventional features are defined below.

Table 18.2. Recommended[a] values of bin width and smoothing for typical histograms

	Peak width[b,c]	Bin width[d]	Smoothing[e]	Peak height[b]
MTR	10 pu	0.1–0.2 pu	0.5 pu	10 % vol/pu
T_1	200 ms[g]	1–5 ms[i]	10 ms	0.17 % vol/ms
MD[f]	0.5×10^{-9} m^2/s[h]	$0.005–0.01 \times 10^{-9}$ m^2/s	0.02×10^{-9} m^2/s	200×10^9 % vol/m^{-2} s

[a] These are for optimal characterization of the peak; advanced global techniques (LDA and PCA) may tolerate and even prefer lower resolution histograms.
[b] Approximate values for whole brain; exact values depend on data acquisition and segmentation.
[c] Full-width half-maximum.
[d] Chosen as approximately 1–2 % of the peak width.
[e] Chosen as 5 % of the peak width; the width of a median filter as used in Figure 11.8 is given; other filters of equivalent width could be used.
[f] Mean diffusivity, $\overline{D}$.
[g] White matter peak at 715 ms (the T_1 histogram is bimodal–see Figure 18.3).
[h] Equal to 0.5×10^{-3} mm^2/s (see Figure 18.2 and Chapter 7). The units for diffusion given in the table (m^2/s) are SI.
[i] A bin width of 1 ms is convenient, although unnecessarily small.

18.4.7.1 Peak Height

Let $\underline{h}^p = \{h_1^p, \ldots, h_N^p\}$ be histogram p where N is the number of bins. h_i^p is the peak height (PH) of histogram p if and only if

$$h_i^p \geq h_j^p, \quad j \neq i, \quad j = 1, \ldots, N \tag{18.5}$$

(h_i^p-is the mode or most common x-value).

18.4.7.2 Peak Location

i is the bin number of the peak, or the peak location, of histogram p if and only if h_i^p is the peak height of the histogram. The x-value at the bin centre is given by Equation (18.2). If more than one bin has a value equal to the peak value, a more subtle approach is needed to find the peak location.

18.4.7.3 Centile Values X_{25} Etc.

These are convenient ways of characterizing the tails of a histogram. The nth centile of a distribution is the x-value where $n\,\%$ of the voxels (or histogram area) lie to the left of the bin. x_{25} is sensitive to structure in the left-hand side of the histogram (where lesions tend to lie,[8] in an MTR histogram). x refers to the MR parameter, so the 25th centile may be MTR_{25}, Dbar_{25} etc. The 25th centile is defined as follows, with similar expressions for other centiles (25th, 50th and 75th centile values have traditionally been used; van Buchem *et al.*, 1997). k is the bin number of the 25th centile of histogram p if and only if k is the largest value which satisfies the following criterion:

$$\sum_{i=1}^{k} h_i^p \leq (25\,\%) \sum_{j=1}^{N} h_j^p \tag{18.6}$$

The centre of bin k, x_{25}, is determined from k using Equation (2).

[8] Other parameters such as T_1 and $\overline{D}$ have histograms where the direction of pathology is reversed, in the sense that CSF and tissue that has partially lost its structure have abnormally *high* values of T_1 or D, so those voxels lie to the right-hand side of the histogram (see Figure 18.4).

18.4.7.4 Mean Parameter Value

The mean parameter (i.e. $\overline{x}$) value is

$$\overline{x} = \sum_{j=1}^{N} x_j h_j^p \Big/ \sum_{j=1}^{N} h_j^p \tag{18.7}$$

where x_j is the value of the parameter at the centre of the jth bin. Note that this can be calculated without generating the histogram, since it is the mean value of all the voxels represented in the histogram, and is routinely carried out in ROI analysis.

18.4.8 Curve Fitting for Bimodal Histogram Features

Bimodal histograms (see Figures 18.3 and 18.14) cannot be well characterized by the unimodal features of the previous section, since overlap of the underlying broad structures prevents them being characterized independently of each other. An alternative approach is to fit the histogram to the sum of several distributions described by analytic functions (e.g. gaussians; Hofman *et al.*, 1999). Each peak then has an effective height, location and width corresponding to the fitted function. This approach is also available for characterizing unimodal histograms. It has the advantage of being less dependent on the exact histogram structure at the peak bin, since the fitting is carried out over all the bins in the locality of the peak. A peak lying between two bin centres can easily be characterized, which may be helpful if it was not possible to form the histogram with small bin width. It can be seen as combining interpolation (since sub-bin resolution is achieved) with smoothing (since several bins may contribute to characterizing a peak), depending on the number of bins over which the fitting is carried out (i.e. the support or width of the gaussian). The characterizing of spectroscopy peaks, that often overlap, has received much attention (see Chapter 9), and there are probably lessons to be learnt from that area.

18.4.9 Global Features – Linear Discriminant Analysis and Principle Component Analysis

The features described so far[9] operate at a particular part of the histogram, often the peak. They are local descriptors. Here the use of global[10] features using advanced techniques is introduced, specifically linear discriminant analysis (LDA) and principle component analysis (PCA). Histogram features (or any other MR parameters measured in disease) have often been tested for clinical relevance, at least in the context of MS and the desire to find MR surrogates for clinical progression and response to treatment, in two ways. First, statistically significant differences between disease subgroups have been looked for, using Student's *t*-test methodology. Second, correlations with disease severity (EDSS[11] in MS) have been measured, in the hope that a high correlation indicates the clinical relevance of the MR parameter. Dehmeshki *et al*. (2002b) has argued that a single (localized) histogram feature cannot be simultaneously optimal for these two distinct tasks, and that selecting from the range of conventional features (peak height, peak location etc., see list above) is unsatisfactory, since it leads to multiple comparisons and loss of sensitivity through the Bonferroni correction. Instead he proposed that LDA is optimal for maximizing the separation between groups of subjects (such as sub-groups of MS), and that it should be seen as a classification problem where the success of *classifying individual subjects* (rather than the separation of groups) should be the prime measure, particularly when some features can separate the groups with very low *p*-values (see Figure 18.9 and Tables 18.3 and 18.4). He proposed that PCA is optimal for correlation with disease severity (such as EDSS), as it captures the within-class variance. As well as measuring correlation coefficients for various features, the concept was extended to measuring their predictive

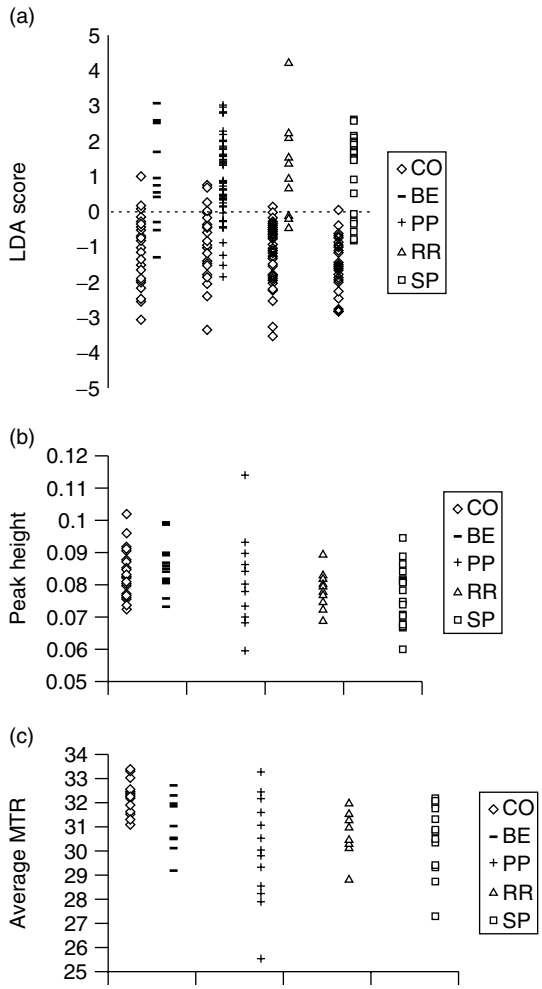

Figure 18.9. (a) Scatter plot for LDA scores derived from MTR histograms of normal controls (CO) and people with MS (subgroups BE, PP, RR, SP). Individual subjects could be classified between CO and RR, or CO and SP, solely on the basis of their histogram, with high success rates (45/49 and 50/55, respectively). Note that as the LDA scores relate to *binary* comparisons, each control has a different score according to which comparison is being made. (b) and (c) In contrast, conventional histogram features give largely overlapping distributions. Adapted with permission from Dehmeshki *et al*. 2002b with revision

[9] The mean parameter value does not operate at a particular location in the histogram, yet it can easily be calculated once the segmentation has been performed, without the need to create a histogram, and hardly qualifies as a 'histogram parameter'.

[10] *Global* is used here to mean 'all of the histogram' (as distinct to 'all of the brain').

[11] *EDSS*: Extended Disability Status Scale, used to characterize disability in MS (Kurtzke, 1983).

Table 18.3. Performance of LDA score and conventional MTR histogram parameters in separating and classifying active NPSLE from the other groups. Reproduced with permission from Dehmeshki, J., van Buchem, M.A., Bosma, G.P., Huizinga, T.W., and Tofts, P.S., Systemic lupus erythematosus: diagnostic application of magnetization transfer ratio histograms in patients with neuropsychiatric symptoms – initial results, in *Radiology*. Copyright 2002. Separation using Student's t-test. p-values are shown. Note that the MDA p-values are always lower than those achieved by any other parameters, usually by a large factor

Acute NPSLE	LDA score	Conventional parameters		
		Peak height	Peak location	Mean value
Chronic NPSLE	7×10^{-6}	0.02	0.0001	3×10^{-5a}
Non-NPSLE	2×10^{-13}	5×10^{-6}	3×10^{-6a}	7×10^{-6}
MS	1×10^{-5}	NS	0.0004	0.0002^a
Control	2×10^{-13}	2×10^{-6}	8×10^{-8a}	6×10^{-7}

[a]Best of the three conventional parameters.

Table 18.4. Performance of LDA score and conventional MTR histogram parameters in separating and classifying active NPSLE from the other groups. Reproduced with permission from Dehmeshki, J., van Buchem, M.A., Bosma, G.P., Huizinga, T.W., and Tofts, P.S., Systemic lupus erythematosus: diagnostic application of magnetization transfer ratio histograms in patients with neuropsychiatric symptoms – initial results, in *Radiology*. Copyright 2002. Separation using Student's t-test. p-values are shown. Note that the MDA p-values are always lower than those achieved by any other parameters, usually by a large factor Rates of correct binary classification using LDA

	Acute NPSLE	Chronic NPSLE	Non-NPSLE	MS
Acute NPSLE	NA	NA	NA	NA
Chronic NPSLE	17/19	NA	NA	NA
Non-NPSLE	19/19	17/20	NA	NA
MS	17/19	12/20	18/20	NA
Controls	19/19	17/20	15/20	18/20

Data shown are number of successes/total number of subjects in the two groups.
NS, not significant; NA, not applicable; SLE, systemic lupus erythematosus; NPSLE, neuropsychiatric SLE.

value[12] (Dehmeshki *et al*., 2001; (see Figure 18.9). The eigenvectors coming from the PCA give information on the clinically relevant parts of the histogram (see Figure 18.10).

18.4.9.1 PCA for Correlation and Prediction

The principal components (Webb, 1999) of the covariance matrix of histograms are computed by treating the histograms as replicates of a N-variate observation (N is the number of bins in each histogram). The principal components are uncorrelated with each other and are ordered in decreasing proportion of variation present in all of the original histograms.

Principal components capture the characteristic significant variations for each of the histogram groups. These characteristic variations are in the form of eigenvalues and eigenvectors evaluated from the histogram data. The process of evaluating

[12] *Prediction* is used in the sense of 'can an MR measurement tell us what the current clinical measure is?'. There is no implication here of modelling the future behaviour.

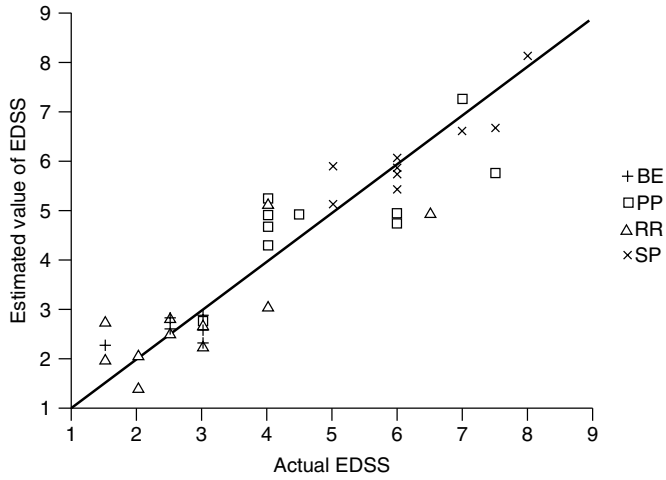

Figure 18.10. Correlation of EDSS with principle components enables a 'predicted EDSS' to be calculated for each subgroup of people with MS, solely from the MTR histogram and knowledge of the subgroup. These are usually within 1 point of the actual clinically measured EDSS value. Compared with conventional features, PCA gives better correlation coefficients. Reproduced with permission from Dehmeshki, J., Ruto, A.C., Arridge, S., Silver, N.C., Miller, D.H. and Tofts, P.S., Analysis of MTR histograms in multiple sclerosis using principal components and multiple discriminant analysis, in *Magn. Reson. Med.*, © 2001 John Wiley & Sons Inc.

the eigenvalues and eigenvectors is as follows. Firstly, the covariance matrix w of n histograms, $\underline{h}^p = \{h_1^p, \ldots, h_N^p\}$ is evaluated:

$$w_{k,l} = w_{l,k} = \frac{1}{n} \sum_p (h_k^p - \overline{h}_k)(h_l^p - \overline{h}_l) \quad (18.8)$$

where

$$\overline{h}_k = \frac{1}{n} \sum_p h_k^p; \quad \overline{h}_l = \frac{1}{n} \sum_p h_l^p$$

Eigenvalues λ and eigenvectors $\underline{v} = (v_1, v_2, \ldots, v_N)$ of this matrix are evaluated:

$$W \cdot \underline{v} = \lambda \underline{v} \quad (18.9)$$

The m most significant (largest) eigenvalues λ_j ($j = 1, m$) and their corresponding eigenvectors are selected to characterize the variation of each patient group. The percentage variation $[PV(m)]$ covered by these m significant components is calculated as follows:

$$PV(m) = \frac{\sum_{j=1}^{m} \lambda_j}{\sum_{j=1}^{N} \lambda_j} \times 100\,\% \quad (18.10)$$

The percentage variation allows us to choose the number of PCs (m) to be used for our further MTR histogram analysis. Note that the principal components, PC, of each histogram are linear combinations (dot products) of the eigenvectors and the histogram.

$$PC = \underline{v}\,\underline{\mathrm{h}}^{\mathrm{p}} = v_1 h_1^p + v_2 h_2^p + \cdots + v_N h_N^p$$

Thus there is a single eigenvector for the whole group of subjects, and individual principle component values for each member of the group.

18.4.9.2 LDA for Group Separation and Classification

The aim of MDA is to maximize the ratio of the between-group variance to the within-group variance. MDA is used to create a nearest-mean-group

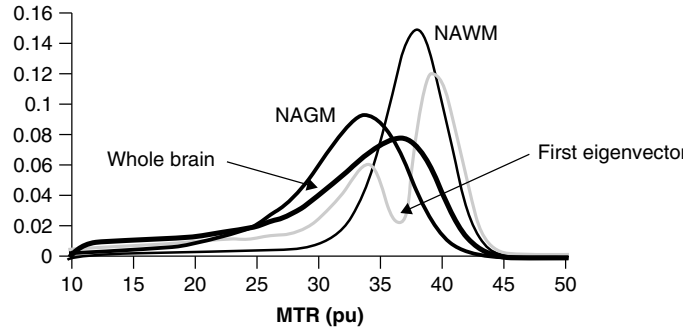

Figure 18.11. The eigenvectors from PCA can give insight into which parts of the histogram are providing important information. PCA of MTR histograms from people with MS shows peaks in the first eigenvector close to those seen in pure normal-appearing grey and white matter. PCA was carried out on whole-brain histograms, yet it appears sensitive to specific changes in grey and white tissues, without the need to formally segment the brain into NAGM and NAWM. Reproduced with permission from Dehmeshki, J., Chard, D.T., Leary, S., Thompson, A.J., Miller, D.H. and Tofts, P.S., Magnetisation transfer histograms in primary progressive multiple sclerosis: grey matter changes relate to disability and principal components analysis shows this most sensitivity, in *Proc. Int. Soc. Magn. Reson. Med.* Copyright 2002 ISMRM

classifier. A brief summary of the techniques is given here, but for more detail see Webb (1999). The aim of LDA is to maximize:

$$\frac{|\tilde{W}_\mathrm{b}|}{|\tilde{W}_\mathrm{w}|} = \frac{|\phi^\mathrm{t} W_\mathrm{b} \phi|}{|\phi^\mathrm{t} W_\mathrm{w} \phi|} \tag{18.11}$$

In this equation, W_b is the between-class scatter matrix, W_w is the within-class scatter matrix, and ϕ is the transformation we are searching for in order to form the optimal discriminant space. We can define the following, with $\underline{h}^{p,i}$ being the histogram of subject p in subgroup i, and n_i being the number of subjects in subgroup i:

$$\overline{\underline{h}}^i = \frac{1}{n_i} \sum_p \underline{h}^{p,i} \tag{18.12}$$

$$\overline{\underline{h}} = \frac{1}{n} \sum_i n_i \overline{\underline{h}}^i \tag{18.13}$$

and

$$W^i = \sum_p (\underline{h}^{p,i} - \overline{\underline{h}}^i)(\underline{h}^{p,i} - \overline{\underline{h}}^i)^\mathrm{t} \tag{18.14}$$

$$W_\mathrm{w} = \sum_i W^i \tag{18.15}$$

$$W_\mathrm{b} = \sum_i n_i (\overline{\underline{h}}^i - \overline{\underline{h}})(\overline{\underline{h}}^i - \overline{\underline{h}})^\mathrm{t} \tag{18.16}$$

Equation (18.12) computes subgroup mean of n_i subjects p in subgroup i. Both the within-class scatter, W_w and the between-class scatter, W_b are analogous to their respective covariance matrices.

In looking for ϕ we can define

$$\underline{y} = \phi^\mathrm{t} \underline{h} \tag{18.17}$$

$$\psi^i \equiv \{\underline{y}^i | \underline{h}^i \in i\text{th group}, \underline{y}^i = \phi^\mathrm{t} \underline{h}^i\}$$

$$\overline{\underline{y}}^i = \frac{1}{n_i} \sum_{\underline{y} \in \psi^i} \underline{y} \tag{18.18}$$

$$\overline{\underline{y}} = \frac{1}{n} \sum_i n_i \overline{\underline{y}}^i \tag{18.19}$$

$$\tilde{W}_\mathrm{w} = \sum_i \sum_{y \in \psi^i} (\underline{y} - \overline{\underline{y}}^i)(\underline{y} - \overline{\underline{y}}^i)^\mathrm{t} \tag{18.20}$$

$$\tilde{W}_\mathrm{b} = \sum_i n_i (\overline{\underline{y}}^i - \overline{\underline{y}})(\overline{\underline{y}}^i - \overline{\underline{y}})^\mathrm{t} \tag{18.21}$$

It follows from this that

$$\tilde{W}_\mathrm{w} = \phi^\mathrm{t} W_\mathrm{w} \phi \tag{18.22}$$

$$\tilde{W}_\mathrm{b} = \phi^\mathrm{t} W_\mathrm{b} \phi \tag{18.23}$$

Taking the determinant of a scatter matrix is equivalent to finding the product of the eigenvalues, which corresponds to the product of the variance. As may be seen with reference to Equation (18.11) by maximizing this ratio, we are looking for a transform ϕ that maximizes the between-class variance with respect to the within-class variance. The solution of Equation (18.11) can be shown to correspond to the generalized eigenvectors of the following Equation:

$$W_{\mathrm{b}}\underline{\phi}_j = \lambda_j W_{\mathrm{w}}\underline{\phi}_j \qquad (18.24)$$

where the vectors $\underline{\phi}_j$ then form the columns of the matrix ϕ.

In addition, the individual dimensions of the discriminant space created by each eigenvector $\underline{\phi}_j$ are now ordered. The between-class variance in dimension j is proportional to the eigenvalue λ_j. Assuming a constant within-class variance, the higher the between-class variance of a dimension, the better the discriminant capacity of that dimension.

One additional step can be taken to scale all the within-class variances to uniform size in the discriminant space. The variance in dimension j can be computed as $\underline{\phi}_j^t W_{\mathrm{w}}\underline{\phi}_j$ and each dimension can be scaled by replacing $\underline{\phi}_j$ with

$$\hat{\underline{\phi}}_j = \frac{\underline{\phi}_j}{\sqrt{\underline{\phi}_j^t W_{\mathrm{w}}\underline{\phi}_j}} \qquad (18.25)$$

giving each new dimension uniform variance. This allows us to use the nearest-mean group classifier, in discriminant space, since this classifier does not account for differing variances between dimensions. The decision as to whether the particular histogram is allocated to one subgroup or another is based on measuring the (Euclidean) distance between its transform scores (created by LDA) and the centroids of all the subgroups in discriminant space.

18.5 WHAT CAN GO WRONG?

18.5.1 Data Collection

Parameter maps may be inaccurate – see the appropriate chapter on how to measure it accurately. Non-uniformity of the transmit (B_1) field will broaden the histogram (for MTR and T_1 but not diffusion). Uncorrected errors in flip angle will shift the histogram in some cases (for example MTR).

18.5.2 Parameter Maps

Parameter maps may suffer from rounding errors, where parameter values are rounded either *down* to the integer value below, or to the *nearest* integer value (which may be up or down). MTR maps, calculated to the nearest 1 pu, are particularly prone to this error. If nearest rounding has been used, then the maximum error is 0.5 pu.[13] If rounding down has been used, the maximum error is 1 pu.

18.5.3 Segmentation

Poor segmentation may include too much CSF, as seen by a large tail in the histogram. A strategy for dealing with partial volume voxels is needed. If a large number are present in the histogram, then atrophy will have an undefined contribution to any changes that are observed.

18.5.4 Histogram Spikes

Histogram spikes may be present. These are quite common in high-resolution histograms, although they are often obscured by smoothing or broad bin-widths (see Figures 18.2, and 18.6). They usually come in pairs (one high, one low), so that a small amount of smoothing attenuates them heavily (see Figure 18.8). The solution (making the images pseudo-continuous by adding noise – see Section 18.4.1) has only recently been discovered.[14] Spikes of a different origin (from mapping errors) may be present if the map contains values that are grossly incorrect, arising for example from movement between the two source images. Diffusion maps sometimes contain so-called 'black pixels' where the calculation has failed.

[13] The root mean square (rms) error for an error distribution that is evenly distributed between 0 and 0.5 pu can be calculated as 0.5 pu/$\sqrt{3}$ = 0.29 pu.

[14] A manuscript by Tozer and Tofts is in preparation.

18.5.5 Bin-Location Ambiguity

In the description given above, labelling a bin by its *centre* (not its left-hand edge) has been advocated. In most published work this bin labelling is not defined. Using a bin edge instead of its centre gives a systematic error of half a bin width. With the use of narrower bins (e.g. 0.1 pu) this potential source of error decreases in magnitude.

18.5.6 Bin Width too Large

Even if the parameter values are available at high enough resolution (e.g. 0.1 pu), the bin width may still be chosen to be too wide (e.g. 1 pu). The values of features such as peak location and height can be very dependent on the bin width and any interpolation that is used (either explicitly on the data or implicitly in the display; see Figure 18.5). MTR histograms typically have a bin width of 1 pu; thus the peak location can be shifted from its true value in a continuous distribution by as much as 0.5 pu. The rms error is 0.3 pu; this is comparable with the shifts seen in disease, and constitutes an avoidable source of random error in the data.

If the bin width is too large, either through choice or because the basic maps are too coarse, *interpolation* will probably help in characterizing the peak. Extra points are created between the measured ones, for example a 1 pu histogram can be interpolated to a resolution of 0.1 pu (Tofts *et al.*, 2001; see Figure 18.12). Interpolation schemes can easily be implemented in a spreadsheet, and there is a large literature on the subject (Press *et al.*, 2002). Spreadsheets often have a facility to 'fill in missing values', although the algorithm used may be undefined. It must be born in mind that the interpolation is essentially guessing the missing values (based on prior information that the histogram is smooth). It is to be hoped that the phenomenon of wide bins is a transient one, that will decline over time as methodology is improved.

18.5.7 Peak Localization and Bimodal Histograms

Some histograms may be bimodal, or at low resolution, in which case the conventional unimodal features are inappropriate, and curve fitting may give better resolution (see Section 18.4.8)

18.5.8 Undefined Histogram Generation

In much published work, very little detail is given on exactly how the histograms were generated. The

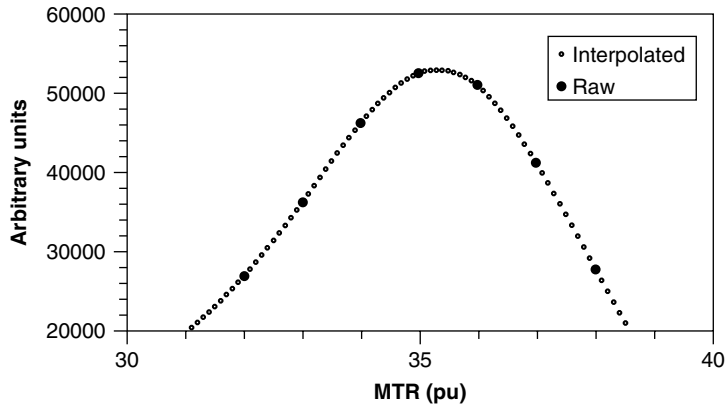

Figure 18.12. Interpolation of a 1 pu MTR histogram (raw) down to 0.1 pu bin width. The interpolation looks realistic, providing appropriate curvature (although its accuracy can only be tested by having actual 0.1 pu data). The peak can be located to within 0.1 pu, at 35.3 pu. Everett's polynomial interpolation scheme (Scheid, 1968), using the values in the neighbouring four bin values (two to the left, and two to the right), was implemented on a PC spreadsheet (available from the author P.T.)

bin width is often not given, and smoothing may be carried out in the display, without being stated. Interpolation may be used when calculating peak location and height, without stating this explicitly. Any peak location value that is given to a precision better than the bin-width must have involved the use of some kind of interpolation (see for example Figure 18.5). Without these details, reproducing histograms across centres, or across an upgrade at a particular centre, is likely to fail.

What to specify when generating a histogram

- Data collection; accuracy of parameter estimates.
- Parameter maps; resolution and rounding.
- Segmentation procedure (including any cut-off in histogram).
- Bin width; location of x-label (centre or edge).
- Smoothing (if any).
- Normalization procedure.
- Feature extraction methods; was any interpolation used?

18.6 CLINICAL APPLICATIONS OF HISTOGRAM ANALYSIS

Histogram analysis allows for the quantification of diffuse pathological change which, in neurological disease, may provide useful insight into underlying disease mechanisms. A good example of where such an approach has been helpful is in MS, although other conditions, namely systemic lupus erythematous, Alzheimer's disease, sickle cell disease, Leber's hereditary optic neuropathy and nocturnal frontal lobe epilepsy, have also been studied in this manner.

MS is of particular interest as the emphasis of study is not only on the focal pathology (the MS lesion or plaque) but also on the diffuse abnormality observable in macroscopically normal tissue (Evangelou *et al*., 2000). Quantitative MR measures including MTR, diffusion and T_1 relaxation time are sensitive to this subtle abnormality and it is in the study of this diffuse change that histogram analysis has been used.

The number and volume of MS lesions correlates only modestly with cumulative disability (Molyneux *et al*., 2001) and this suggests that it is change within the normal-appearing tissue that accounts for much of the burden of disease. Histogram analysis is an ideal way of quantifying this disease burden and it is therefore of no surprise that this overall view shows a stronger relationship with disability than lesion volume measures alone.

An important caveat exists with histogram analysis and this is that with such a global approach, the analysis will include voxels at the brain–CSF interface. Any disease process that leads to cerebral atrophy (as very many neurological diseases do), will result in an increase in the surface area to volume ratio of the brain. CSF has very different MR characteristics to parenchymal brain tissue and so an increase in the relative number of voxels at the brain surface will lead to a change in the histogram. These 'partial' voxels,[15] which contain both CSF and brain parenchyma, have an increasingly dominant role on the histogram as atrophy progresses. It is therefore very important to consider the effects of atrophy when a difference is observed between patient and control groups. Exclusion of the outer portion of the brain from the analysis during the segmentation process may be a reliable way of avoiding this effect (see Figure 18.4 and also Chapter 16 on volume and atrophy)

18.6.1 Multiple Sclerosis: MTR Histograms

A range of studies have been performed in MS using MT histograms. The increasing shift of interest from visible lesions in T_2-weighted images to subtle changes in normal-appearing brain tissue has been largely driven by such analyses. Some studies have shown a significant relationship between histogram metrics and physical disability (Dehmeshki *et al*., 2001; Iannucci

[15] *Partial voxels* is a term used to refer to voxels that contain more than one tissue type, and therefore suffer from partial volume effects.

et al., 1999; van Waesberghe *et al*., 1998), with another (Rovaris *et al*., 1999) showing that correlations also exist between MTR histogram metrics and other MR measures. The use of principle component analysis (Dehmeshki *et al*., 2001) reveals that a better relationship between MTR histogram characteristics and disability is observable [Spearman's rank correlation coefficient (r_s) = 0.8] than when disability is correlated with isolated histogram features. (The correlation between the 25th percentile and disability for instance was $r_s = 0.37$.) Further to the correlation with physical disability, a number of studies have looked at the association between MTR histogram measures and cognitive dysfunction. One study (Rovaris *et al*., 2000a) found that, with multivariate regression, MTR histograms derived from cortical and subcortical brain tissue were the only factor that was associated with cognitive impairment. A further study (Comi *et al*., 1999) found that MS patients with frontal lobe cognitive deficits had abnormal whole brain and frontal lobe histogram metrics while histograms derived from cerebellar tissue were similar to cerebellar histograms derived from MS subjects without cognitive impairment.

A number of studies have looked at the ability of MTR histograms to show differences between MS clinical subgroups. One study (Tortorella *et al*., 2000) has shown that there is a difference between relapsing remitting and secondary progressive patients with the peak height from normal-appearing brain tissue being lower in the latter. A similar finding was found in grey matter segments (Ge *et al*., 2002). It is interesting that, when comparison was made between primary progressive and secondary progressive patients (Rovaris *et al*., 2001), no such difference was found, despite the secondary progressive group having a higher T_2 lesion load. A large cross-sectional study (Filippi *et al*., 1999) showed that patients with a clinically isolated syndrome suggestive of MS and those with benign MS had MTR histograms similar to those of controls. Relapsing–remitting MS subjects had reduced peak heights and mean MTRs while a similar but more severe change was observed in those with secondary progressive disease (Figure 18.13).

Another study (Dehmeshki *et al*., 2001) found similar findings in that benign patients were not significantly different from controls while other subgroups were. Here, MTR histograms were able to discriminate between patients with significant disability and those that were less disabled. An improvement in the relationship to disability was achieved with the use of principle component analysis.

A number of studies have looked at serial data, using histograms to show change over time. One group (Patel *et al*., 1999) have shown a subtle change in MTR peak height (in the order of 5 %), despite the lack of detectable clinical change. Another (Rocca *et al*., 1999) showed that a change in histogram metrics was observable in a group of relapsing–remitting and secondary progressive subjects over a 3 year period. Changes in mean MTR, peak height and the 25th and 50th percentiles were seen in MS subjects (in the order of 5–10 %), whereas no change was observable in controls. A larger study (Filippi *et al*., 2000) showed that there was a change in MTR histogram metrics over a 12 month period in relapsing–remitting and secondary progressive subjects whilst there was no observable change in those with benign and primary progressive disease. Change was also observed in those with a clinically isolated syndrome suggestive of MS.

One of the principle reasons for developing MR measures in MS is to find a marker that correlates well with future disability. If a specific therapy could be shown to reverse change in this measure then it would imply that the agent had real potential in preventing cumulative disability. At present it has yet to be shown that MTR histograms can be used in such a way, although the long-term data are not yet available. One study (Richert *et al*., 1998) has looked at the effect of a disease-modifying drug (beta interferon) on MTR histogram metrics and no change was seen in the metrics during the 8 months of the clinical trial.

A further advantage of histogram analysis is that it is sensitive to subtle change, early on in the disease before lesions are visible, something

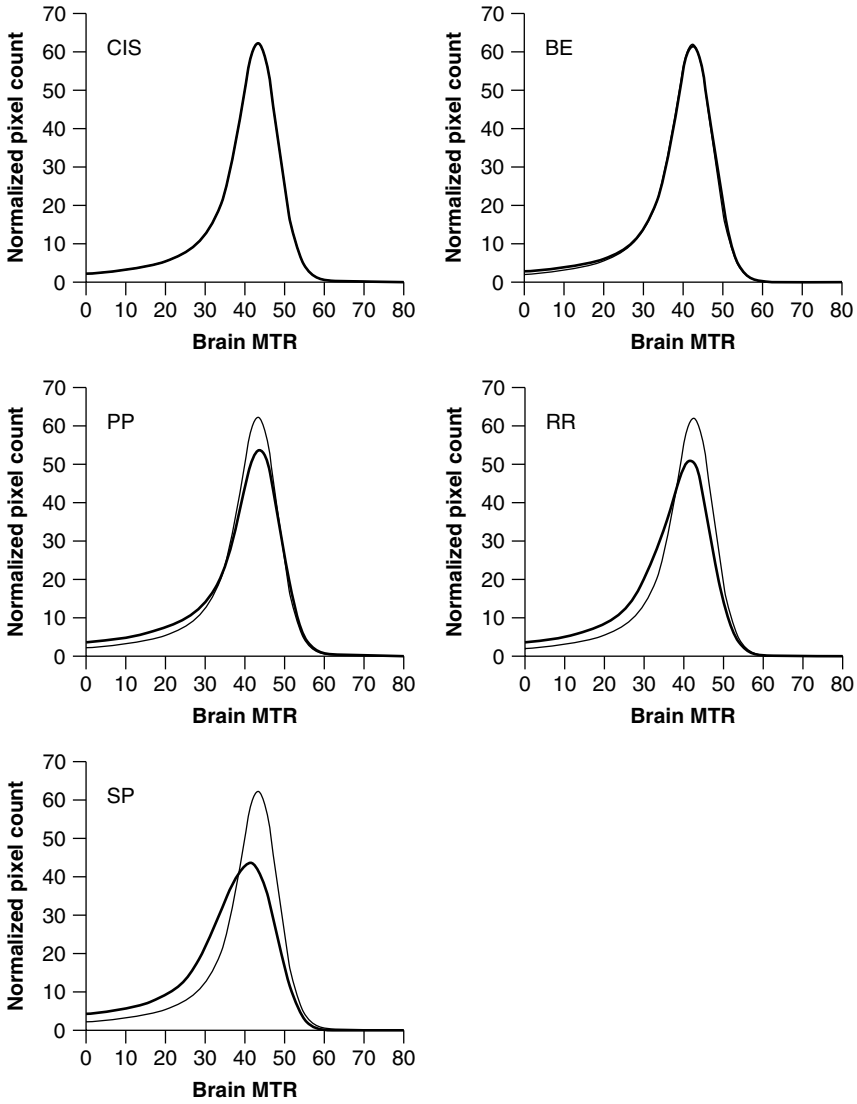

Figure 18.13. MTR whole-brain histograms in MS (black lines) and normal controls (grey lines). Clinically isolated syndromes suggestive of MS (CIS), benign MS (Be), primary progressive MS (PP), relapsing–remitting MS (RR) and secondary progressive MS (SP). The largest abnormality is seen in the MS phenotype that is clinically most severe (SP). Some of this abnormality arises from lesions; smaller effects are seen in normal-appearing brain (Tortorella *et al*., 2000). Reproduced with permission from Filippi, M., Iannucci, G., Tortorella, C., Minicucci, L., Horsfield, M.A., Colombo, B., Sormani, M.P. and Comi, G., Comparison of MS clinical phenotype using conventional and magnetization transfer MRI, in *Neurology*, **55**, 940–946, Copyright 1999 Lippincot•, Williams and Wilkins

that an ROI approach may not detect. Although diffuse cerebral abnormality may be widespread, early in the natural history of neurological disease it is not necessarily homogeneously distributed. For this reason, histogram analysis may be better than an ROI approach at detecting this heterogeneous abnormality. In the case of MS, early diffuse change is apparent, even prior to the onset of the

second clinical episode (by convention, a second attack is necessary before a clinical diagnosis of MS can be made). A study of subjects with a clinically isolated syndrome suggestive of MS has shown MTR abnormality in the normal-appearing tissue using histogram analysis (Iannucci *et al*., 2000). The degree of abnormality was also a predictor of eventual progression to MS. By comparison, a region of interest analysis in subjects with clinically isolated syndromes, was unable to detect abnormality of the normal appearing tissue (Brex *et al*., 2001).

Unaffected relatives of patients with MS have been studied with MTR histogram analysis (Siger-Zajdel *et al*., 2002). Of note, unaffected relatives, none of whom had lesions on conventional imaging, had significantly reduced peak heights when compared with controls. Here histogram analysis can demonstrate abnormality even when it is sufficiently subtle to be subclinical.

18.6.2 Multiple Sclerosis: Diffusion Histograms

Histogram analysis has aided the study of MS using diffusion-weighted imaging, with histograms of the ADC showing right shift and reduced peak height in MS subjects. This change correlated significantly with disability and disease duration, which had not been shown with an ROI approach (Wilson *et al*., 2001). Furthermore, mean diffusivity histograms are abnormal in MS (see Figure 18.2; Cercignani *et al*., 2000) and both mean diffusivity and fractional anisotropy histograms have been shown to correlate with physical disability (Cercignani *et al*., 2001a). Mean diffusivity histograms have demonstrated that normal-appearing white and grey matter in MS (segmented by fractional anisotropy thresholds) is significantly different from controls (Figure 18.4; Cercignani *et al*., 2001a) and MS subgroups can be separated by differences in ADC histogram metrics (Nusbaum *et al*., 2000). It is also interesting that diffusion histogram metrics are not correlated with MTR histogram metrics in relapsing–remitting MS (Iannucci *et al*., 2001a), suggesting that the two measures are, at least partially, independent.

18.6.3 Multiple Sclerosis: T_1 Histograms

Comparatively few groups have studied MS with the use of T_1 histograms. An analysis of total white matter T_1 (Vaithianathar *et al*., 2002) confirmed that T_1 is abnormal in MS white matter and that T_1 histogram metrics correlate with atrophy and T_2 lesion load measures. Further work (Griffin *et al*., 2002) has shown that there is little difference between whole brain and normal-appearing tissue histograms, suggesting that much of the observed abnormality arises from normal-appearing tissue. A correlation was also shown between histogram metrics and upper limb function.

18.6.4 Other Diseases Studied with Histograms

A range of other neurological conditions have been studied using histogram analysis. The hereditary condition CADASIL (cerebral autosomal dominant arteriopathy with subcortical infarcts and leukencephalopathy) in just one example (Iannucci *et al*., 2001b). Here, the average MTR and peak location from the whole brain and normal-appearing brain tissue histograms significantly differed between patients and controls. The whole brain histograms were more markedly abnormal than the normal-appearing brain histograms, indicating that CADASIL lesions were having a significant impact on the overall burden of disease.

Alzheimer's disease has also been studied using both mean diffusivity and MTR histograms (Bozzali *et al*., 2001). Here, peak height for both parameters in cortical grey matter was abnormally low on comparison of patients with controls. Although this difference may have been explained by partial volume effects secondary to atrophy, the study revealed detectable abnormality in the temporal lobe but not in the occipital cortex.

Similarly, nocturnal frontal lobe epilepsy (NFLE), an autosomal dominant disorder, has been studied with mean diffusivity and MTR histogram analysis (Ferini-Strambi *et al*., 2000). In this case, peak heights for mean diffusivity and MTR

histograms were significantly reduced in NFLE subjects despite the lack of evidence for detectable abnormality in subjects with idiopathic generalized epilepsy. It was suggested that the findings indicate a diffuse, widespread abnormality, a concept supported by the lack of detectable MTR and mean diffusivity difference between frontal and non-frontal brain tissue

Cerebral autoimmunity other than MS has also been investigated with histogram measures, not least in an attempt to provide MR measures that distinguish MS from other immune mediated disease. Systemic lupus erythematosus (SLE) may often resemble MS on conventional imaging, although one group (Rovaris *et al.*, 2000b) has shown some success in discriminating between MS and SLE on the basis of MTR histogram metrics. Other workers (Bosma *et al.*, 2000; Dehmeshki *et al.*, 2002c) found that MTR histogram metrics could distinguish between subtypes of neuropsychiatric SLE and that discriminatory power can be improved with multivariate discriminate analysis.

T_1 histograms have been used to quantify diffuse cerebral abnormality in sickle cell disease (Steen *et al.*, 1998). In this condition, clinical measures of subtle cognitive impairment reveal abnormality even in those with normal conventional imaging. This study demonstrated that, in those with conventional imaging, T_1 histograms were abnormal supporting these clinical findings.

Leber's hereditary optic neuropathy (LHON) is a mitochondrial condition that results in optic atrophy and it is perhaps surprising that normal-appearing brain MTR and mean diffusivity histograms are both abnormal (Inglese *et al.*, 2001). This possibly indicates that there is diffuse, albeit subclinical, abnormality in cerebral tissue which only manifests itself as disease of the optic nerve.

Finally, normal aging has been studied with both MTR and diffusion histogram metrics. ADC histograms were right-shifted with lower peaks in older healthy controls (Nusbaum *et al.*, 2000), while mean histogram MTR was negatively correlated with age (Tanabe *et al.*, 1997)

18.7 CONCLUSIONS – THE FUTURE OF HISTOGRAMS

Histogram analysis is a powerful aid to the study of neurological disease. Not only is it able to provide an overall measure of disease burden yet it can also detect subtle, diffuse change early in the course of an illness. At present, most of the work has centred on two quantitative measures, MTR and diffusion, yet there is potential to extend histogram analysis to other parameters. The high sensitivity of global features of MTR histograms suggests new ways of using MR parameters to predict future clinical status, and to classify individual patients into disease subgroups There is also scope to study a much wider range of neurological disease where diffuse abnormalities are suspected.

The optimum methodologies for histogram generation and analysis are still to be identified. Under some conditions a bimodal MTR histogram can be obtained, with good separation of the white and grey matter peaks (Figure 18.14); this clearly holds the potential for greater specificity without the need for segmentation. It is possible that a high spatial resolution acquisition and histogram of a part of the brain that is sensitive to diffuse changes may be at least as useful as a whole-brain histogram. The optimum voxel size is still to be investigated. A reduction in voxel size would reduce partial volume effects, giving higher resolution histograms with more structural detail and less contribution from atrophy. This is evident in the T_1 histogram (Figure 18.3). Clearly, noise will limit how far we can move in this direction. Improved uniformity of parameter maps will give histograms that show more structure of biological origin. The contribution of the advanced global techniques (LDA and PCA) is yet to be evaluated; the emphasis on peak characterization is likely to decrease, particularly for structured histograms such as T_1, and data collection strategies may be altered to optimize the benefit of this analysis paradigm.

Acknowledgements

Test data for Figure 18.12 on interpolation were provided by Dr Stefan Steens.

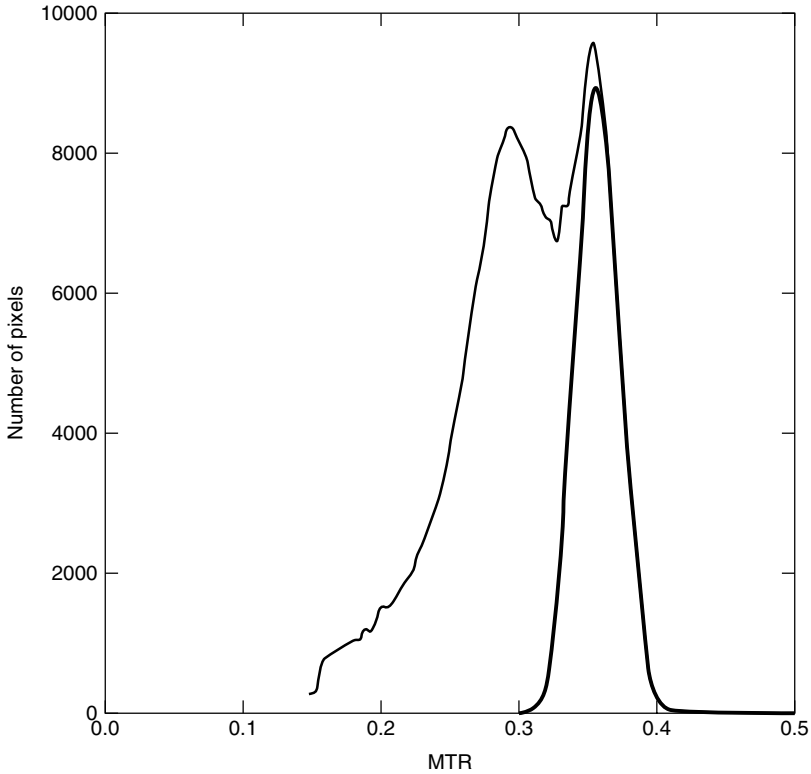

Figure 18.14. MTR histograms from most of the brain (thin line), and from segmented white matter (thick line). The brain histogram is bimodal, with peaks corresponding to grey matter (left-hand side) and white matter (right-hand side). The reason for this being bimodal, when others have found unimodal MTR histograms, is unclear. The reason may lie in the use of a spin echo sequence [although Barker *et al*., (1996) also used a spin echo sequence], in the particular way the saturation was carried out (the body coil was used for transmission, which gives a more uniform RF field and less broadening of the histogram), in the use of coronal slices or the omission of some posterior brain tissue. Reproduced with permission from Hofman, P.A., Kemerink, G.J., Jolles, J. and Wilmink, J.T., Quantitative analysis of magnetization transfer images of the brain: effect of closed head injury, age and sex on white matter, *Magn. Reson. Med.* Copyright 1999 John Wiley & Sons Inc

REFERENCES

Barker, G. J., Tofts, P. S. and Gass, A. 1996, An interleaved sequence for accurate and reproducible clinical measurement of magnetization transfer ratio, *Magn. Reson. Imag.*, **14**, 403–411.

Bosma, G. P., Rood, M. J., Huizinga, T. W., de Jong, B. A., Bollen, E. L. and van Buchem, M. A. 2000, Detection of cerebral involvement in patients with active neuropsychiatric systemic lupus erythematosus by the use of volumetric magnetization transfer imaging, *Arthritis Rheum.*, **43**, 2428–2436.

Bozzali, M., Franceschi, M., Falini, A., Pontesilli, S., Cercignani, M., Magnani, G., Scotti, G., Comi, G. and Filippi, M. 2001, Quantification of tissue damage in AD using diffusion tensor and magnetization transfer MRI, *Neurology*, **57**, 1135–1137.

Brex, P. A., Leary, S. M., Plant, G. T., Thompson, A. J. and Miller, D. H. 2001, Magnetization transfer imaging in patients with clinically isolated syndromes suggestive of multiple sclerosis, *Am. J. Neuroradiol.*, **22**, 947–951.

Cercignani, M., Iannucci, G., Rocca, M. A., Comi, G., Horsfield, M. A. and Filippi, M. 2000, Pathologic damage in MS assessed by diffusion-weighted and magnetization transfer MRI, *Neurology*, **54**, 1139–1144.

Cercignani, M., Inglese, M., Pagani, E., Comi, G. and Filippi, M. 2001a, Mean diffusivity and fractional anisotropy histograms of patients with multiple sclerosis, *Am. J. Neuroradiol.*, **22**, 952–958.

Cercignani, M., Bozzali, M., Iannucci, G., Comi, G. and Filippi, M. 2001b, Magnetisation transfer ratio and mean diffusivity of normal appearing white and grey matter from patients with multiple sclerosis, *J. Neurol. Neurosurg. Psychiat.*, **70**, 311–317.

Comi, G., Rovaris, M., Falautano, M., Santuccio, G., Martinelli, V., Rocca, M. A., Possa, F., Leocani, L., Paulesu, E. and Filippi, M. 1999, A multiparametric MRI study of frontal lobe dementia in multiple sclerosis, *J. Neurol. Sci.*, **171**, 135–144.

Dehmeshki, J., Ruto, A. C., Arridge, S., Silver, N. C., Miller, D. H. and Tofts, P. S. 2001, Analysis of MTR histograms in multiple sclerosis using principal components and multiple discriminant analysis, *Magn. Reson. Med.*, **46**, 600–609.

Dehmeshki, J., Chard, D. T., Leary, S., Thompson, A. J., Miller, D. H. and Tofts, P. S. 2002a, Magnetisation transfer histograms in primary progressive multiple sclerosis: grey matter changes relate to disability and principal components analysis shows this most sensitively, *Proc. Int. Soc. Magn. Reson. Med.*, **10**, 179.

Dehmeshki, J., Barker, G. J. and Tofts, P. S. 2002b, Classification of disease subgroup and correlation with disease severity using magnetic resonance imaging whole-brain histograms: application to magnetization transfer ratios and multiple sclerosis, *IEEE Trans. Med. Imag.*, **21**, 320–331.

Dehmeshki, J., van Buchem, M. A., Bosma, G. P., Huizinga, T. W. and Tofts, P. S. 2002c, Systemic lupus erythematosus: diagnostic application of magnetization transfer ratio histograms in patients with neuropsychiatric symptoms – initial results, *Radiology*, **222**, 722–728.

Evangelou, N., Konz, D., Esiri, M. M., Smith, S., Palace, J. and Matthews, P. M. 2000, Regional axonal loss in the corpus callosum correlates with cerebral white matter lesion volume and distribution in multiple sclerosis, *Brain*, **123** (Pt 9), 1845–1849.

Ferini-Strambi, L., Bozzali, M., Cercignani, M., Oldani, A., Zucconi, M. and Filippi, M. 2000, Magnetization transfer and diffusion-weighted imaging in nocturnal frontal lobe epilepsy, *Neurology*, **54**, 2331–2333.

Filippi, M., Iannucci, G., Tortorella, C., Minicucci, L., Horsfield, M. A., Colombo, B., Sormani, M. P. and Comi, G. 1999, Comparison of MS clinical phenotypes using conventional and magnetization transfer MRI, *Neurology*, **52**, 588–594.

Filippi, M., Inglese, M., Rovaris, M., Sormani, M. P., Horsfield, P., Iannucci, P. G., Colombo, B. and Comi, G. 2000, Magnetization transfer imaging to monitor the evolution of MS: a 1-year follow-up study, *Neurology*, **55**, 940–946.

Ge, Y., Grossman, R. I., Udupa, J. K., Babb, J. S., Mannon, L. J. and McGowan, J. C. 2002, Magnetization transfer ratio histogram analysis of normal-appearing gray matter and normal-appearing white matter in multiple sclerosis, *J. Comput. Assist. Tomogr.*, **26**, 62–68.

Griffin, C. M., Dehmeshki, J., Chard, D. T., Parker, G. J., Barker, G. J., Thompson, A. J., Miller, D. H. 2002, T_1 histograms of normal-appearing brain tissue are abnormal in early relapsing–remitting multiple sclerosis. *Mult. Scles.* **8**, 211–216.

Hofman, P. A., Kemerink, G. J., Jolles, J. and Wilmink, J. T. 1999, Quantitative analysis of magnetization transfer images of the brain: effect of closed head injury, age and sex on white matter, *Magn. Reson. Med.*, **42**, 803–806.

Iannucci, G., Minicucci, L., Rodegher, M., Sormani, M. P., Comi, G. and Filippi, M. 1999, Correlations between clinical and MRI involvement in multiple sclerosis: assessment using $T(1)$, $T(2)$ and MT histograms, *J. Neurol. Sci.*, **171**, 121–129.

Iannucci, G., Tortorella, C., Rovaris, M., Sormani, M. P., Comi, G. and Filippi, M. 2000, Prognostic value of MR and magnetization transfer imaging findings in patients with clinically isolated syndromes suggestive of multiple sclerosis at presentation, *Am. J. Neuroradiol.*, **21**, 1034–1038.

Iannucci, G., Rovaris, M., Giacomotti, L., Comi, G. and Filippi, M. 2001a, Correlation of multiple sclerosis measures derived from T_2-weighted, T_1-weighted, magnetization transfer and diffusion tensor MR imaging, *Am. J. Neuroradiol.*, **22**, 1462–1467.

Iannucci, G., Dichgans, M., Rovaris, M., Bruning, R., Gasser, T., Giacomotti, L., Yousry, T. A. and Filippi, M. 2001b, Correlations between clinical findings and magnetization transfer imaging metrics of tissue damage in individuals with cerebral autosomal dominant arteriopathy with subcortical infarcts and leukoencephalopathy, *Stroke*, **32**, 643–648.

Inglese, M., Rovaris, M., Bianchi, S., La Mantia, L., Mancardi, G. L., Ghezzi, A., Montagna, P., Salvi, F. and Filippi, M. 2001, Magnetic resonance imaging, magnetisation transfer imaging and diffusion weighted imaging correlates of optic nerve, brain and cervical cord damage in Leber's hereditary optic neuropathy, *J. Neurol. Neurosurg. Psychiat.*, **70**, 444–449.

Kurtzke, J. F. 1983, Rating neurologic impairment in multiple sclerosis: an expanded disability status scale (EDSS), *Neurology*, **33**, 1444–1452.

Molyneux, P. D., Barker, G. J., Barkhof, F., Beckmann, K., Dahlke, F., Filippi, M., Ghazi, M., Hahn, D., MacManus, D., Polman, C., Pozzilli, C., Kappos, L., Thompson, A. J., Wagner, K., Yousry, T. and Miller, D. H. 2001, Clinical-MRI correlations in a European trial of interferon beta-1b in secondary progressive MS, *Neurology*, **57**, 2191–2197.

Nusbaum, A. O., Tang, C. Y., Wei, T., Buchsbaum, M. S. and Atlas, S. W. 2000, Whole-brain diffusion MR histograms differ between MS subtypes, *Neurology*, **54**, 1421–1427.

Parker, G. J., Barker, G. J. and Tofts, P. S. 2001, Accurate multislice gradient echo T(1) measurement in the presence of non-ideal RF pulse shape and RF field nonuniformity, *Magn. Reson. Med.*, **45**, 838–845.

Patel, U. J., Grossman, R. I., Phillips, M. D., Udupa, J. K., McGowan, J. C., Miki, Y., Wei, L., Polansky, M., van Buchem, M. A. and Kolson, D. 1999, Serial analysis of magnetization-transfer histograms and Expanded Disability Status Scale scores in patients with relapsing-remitting multiple sclerosis, *Am. J. Neuroradiol.*, **20**, 1946–1950.

Press, W. H., Teukolsky, S. A., Vettering, W. T. and Flannery, B. P. (eds) 2002, *Numerical Recipes in C++: The Art of Scientific Computing*, 2nd edn. Cambridge University Press, Cambridge.

Richert, N. D., Ostuni, J. L., Bash, C. N., Duyn, J. H., McFarland, H. F. and Frank, J. A. 1998, Serial whole-brain magnetization transfer imaging in patients with relapsing-remitting multiple sclerosis at baseline and during treatment with interferon beta-1b, *Am. J. Neuroradiol.*, **19**, 1705–1713.

Rocca, M. A., Mastronardo, G., Rodegher, M., Comi, G. and Filippi, M. 1999, Long-term changes of magnetization transfer-derived measures from patients with relapsing-remitting and secondary progressive multiple sclerosis, *Am. J. Neuroradiol.*, **20**, 821–827.

Rovaris, M., Bozzali, M., Rodegher, M., Tortorella, C., Comi, G. and Filippi, M. 1999, Brain MRI correlates of magnetization transfer imaging metrics in patients with multiple sclerosis, *J. Neurol. Sci.*, **166**, 58–63.

Rovaris, M., Filippi, M., Minicucci, L., Iannucci, G., Santuccio, G., Possa, F. and Comi, G. 2000a, Cortical/subcortical disease burden and cognitive impairment in patients with multiple sclerosis, *Am. J. Neuroradiol.*, **21**, 402–408.

Rovaris, M., Viti, B., Ciboddo, G., Gerevini, S., Capra, R., Iannucci, G., Comi, G. and Filippi, M. 2000b, Brain involvement in systemic immune mediated diseases: magnetic resonance and magnetisation transfer imaging study, *J. Neurol. Neurosurg. Psychiat.*, **68**, 170–177.

Rovaris, M., Bozzali, M., Santuccio, G., Ghezzi, A., Caputo, D., Montanari, E., Bertolotto, A., Bergamaschi, R., Capra, R., Mancardi, G., Martinelli, V., Comi, G. and Filippi, M. 2001, *In vivo* assessment of the brain and cervical cord pathology of patients with primary progressive multiple sclerosis, *Brain*, **124**(Pt 12), 2540–2549.

Scheid, F. 1968, *Schaum's Outline of Theory and Problems of Numerical Analysis.* McGraw-Hill, New York.

Siger-Zajdel, M., Filippi, M. and Selmaj, K. 2002, MTR discloses subtle changes in the normal-appearing tissue from relatives of patients with MS, *Neurology*, **58**, 317–320.

Steen, R. G., Reddick, W. E., Mulhern, R. K., Langston, J. W., Ogg, R. J., Bieberich, A. A., Kingsley, P. B. and Wang, W. C. 1998, Quantitative MRI of the brain in children with sickle cell disease reveals abnormalities unseen by conventional MRI, *J. Magn. Reson. Imag.*, **8**, 535–543.

Tanabe, J. L., Ezekiel, F., Jagust, W. J., Schuff, N. and Fein, G. 1997, Volumetric method for evaluating magnetization transfer ratio of tissue categories: application to areas of white matter signal hyperintensity in the elderly, *Radiology*, **204**, 570–575.

Tofts, P. S., Steens, S. C. A., Dehmeshki, J., Hofman, P., van Waesberghe, J. H. and van Buchem, M. A. 2001, Matching MTR histograms for multicentre studies., *Proc. Int. Soc. Magn. Reson. Med.*, **2**, 1380.

Tortorella, C., Viti, B., Bozzali, M., Sormani, M. P., Rizzo, G., Gilardi, M. F., Comi, G. and Filippi, M. 2000, A magnetization transfer histogram study of normal-appearing brain tissue in MS, *Neurology*, **54**, 186–193.

Vaithianathar, L., Terch, C. R., Morgan, P. S., Wilson, M. and Blumhardt, L. D. 2002, T_1 relaxation time mapping of white matter tracts in multiple sclerosis defined by diffusion tensor imaging. *J. Neurol.*, **249**, 1272–1278.

van Buchem, M. A., McGowan, J. C., Kolson, D. L., Polansky, M. and Grossman, R. I. 1996, Quantitative volumetric magnetization transfer analysis in multiple sclerosis: estimation of macroscopic and microscopic disease burden, *Magn. Reson. Med.*, **36**, 632–636.

van Buchem, M. A., Udupa, J. K., McGowan, J. C., Miki, Y., Heyning, F. H., Boncoeur-Martel, M. P., Kolson, D. L., Polansky, M. and Grossman, R. I.

1997, Global volumetric estimation of disease burden in multiple sclerosis based on magnetization transfer imaging, *Am. J. Neuroradiol.*, **18**, 1287–1290.

van Waesberghe, J. H., van Buchem, M. A., Filippi, M., Castelijns, J. A., Rocca, M. A., van der, Polman, C. H. and Barkhof, F. 1998, MR outcome parameters in multiple sclerosis: comparison of surface-based thresholding segmentation and magnetization transfer ratio histographic analysis in relation to disability (a preliminary note), *Am. J. Neuroradiol.*, **19**, 1857–1862.

Webb, A. 1999, *Statistical Pattern Recognition*. Oxford University Press, Oxford.

Wilson, M., Morgan, P. S., Lin, X., Turner, B. P. and Blumhardt, L. D. 2001, Quantitative diffusion weighted magnetic resonance imaging, cerebral atrophy and disability in multiple sclerosis, *J. Neurol. Neurosurg. Psychiat.*, **70**, 318–322.

Queries in Chapter 18:

Q1. Please clarify if ‘Neorol’ is fine or should it be ‘Neurol’.
Q2. Please clarify if ‘Lippincot’ is fine or should it be ‘Lippincott’